Forest Ecosystems 9 (2022) 100065

Contents lists available at ScienceDirect

Forest Ecosystems

journal homepage: www.keaipublishing.com/cn/journals/forest-ecosystems

Ground-based/UAV-LiDAR data fusion for quantitative structure modeling and tree parameter retrieval in subtropical planted forest

Reda Fekry [a], Wei Yao [a,b,*], Lin Cao [c], Xin Shen [c]

[a] Department of Land Surveying and Geo-informatics, The Hong Kong Polytechnic University, Hung Hom, Hong Kong, China
[b] The Hong Kong Polytechnic University Shenzhen Research Institute, Shenzhen, China
[c] Co-Innovation Center for Sustainable Forestry, Nanjing Forestry University, Nanjing, 210037, China

ARTICLE INFO

Keywords:
Ground/aerial view mobile LiDAR
Point cloud
Co-registration
Fusion
QSM
Tree parameter retrieval

ABSTRACT

Light detection and ranging (LiDAR) has contributed immensely to forest mapping and 3D tree modelling. From the perspective of data acquisition, the integration of LiDAR data from different platforms would enrich forest information at the tree and plot levels. This research develops a general framework to integrate ground-based and UAV-LiDAR (ULS) data to better estimate tree parameters based on quantitative structure modelling (QSM). This is accomplished in three sequential steps. First, the ground-based/ULS LiDAR data were co-registered based on the local density peaks of the clustered canopy. Next, redundancy and noise were removed for the ground-based/ULS LiDAR data fusion. Finally, tree modeling and biophysical parameter retrieval were based on QSM. Experiments were performed for Backpack/Handheld/UAV-based multi-platform mobile LiDAR data of a subtropical forest, including poplar and dawn redwood species. Generally, ground-based/ULS LiDAR data fusion outperforms ground-based LiDAR with respect to tree parameter estimation compared to field data. The fusion-derived tree height, tree volume, and crown volume significantly improved by up to 9.01%, 5.28%, and 18.61%, respectively, in terms of *r*RMSE. By contrast, the diameter at breast height (DBH) is the parameter that has the least benefits from fusion, and *r*RMSE remains approximately the same, because stems are already well sampled from ground data. Additionally, particularly for dense forests, the fusion-derived tree parameters were improved compared to those derived from ground-based LiDAR. Ground-based LiDAR can potentially be used to estimate tree parameters in low-stand-density forests, whereby the improvement owing to fusion is not significant.

1. Introduction

Forest management is essential because of forest's multiple roles, including water supply, mitigation of climate change, food production, and extraction of timber and fuelwood (FAO and UNEP, 2020). Trees are one of the most important features of forests, and they change over time as they grow or degrade. Up-to-date information on trees and other forest elements is essential for a comprehensive interpretation of their ecological functions and processes. Light detection and ranging (LiDAR) systems obtain three-dimensional (3D) information with multi-functional details, showing their importance and popularity in forest mapping and management. Depending on the perspective of data acquisition, LiDAR systems can be divided into airborne and ground-based systems. The most widely used LiDAR system is the airborne laser scanning (ALS) system, which mainly features georeferenced data (Polewski and Yao, 2019) to cover inaccessible forest areas with rough terrains or dangerous wildlife. The new generation of ALS utilizes unmanned aerial vehicles (UAVs) as a carrier platform for a laser scanner or simply an unmanned laser scanner (ULS). The ULS is a lightweight system that integrates a laser scanner with a global navigation satellite system/inertial measurement unit (GNSS/IMU) for positioning and orientation. By contrast, a common ground-based platform refers to a terrestrial laser scanner (TLS), which is normally able to provide a point cloud of higher density and more details compared to other LiDAR platforms. The main challenge with the TLS is occlusion effect, in which some distant areas are scanned with a low density or occluded by other objects within the field of view. The main solution to the occlusion problem is the TLS of the multi-scan mode, which functions by integrating two or more scans to reduce the occlusion effect in the resulting point cloud. These scans can be performed in either the static or kinematic mode, or both.

Recently, new advances in lightweight device development have facilitated the emergence of mobile LiDAR platforms such as backpack

* Corresponding author. Department of Land Surveying and Geo-informatics, The Hong Kong Polytechnic University, Hung Hom, Hong Kong, China.
E-mail address: wei.hn.yao@polyu.edu.hk (W. Yao).

https://doi.org/10.1016/j.fecs.2022.100065
Received 3 May 2022; Received in revised form 23 July 2022; Accepted 30 August 2022

laser scanners (BLS) and handheld laser scanners (HLS), where the scanner is carried by a walking operator to acquire high-fidelity on-site point clouds in a kinematic manner. These advances enable the efficient and flexible scanning of impassable areas that cannot be reached by a vehicle (Oveland et al., 2018). In general, each LiDAR system group exhibits advantages and disadvantages with respect to the scanning results. Airborne systems scan to generate overhead observations, providing a high-density point cloud for the (high-level) tree canopy, whereas the lower level has a low-density point cloud. Conversely, ground-based platforms scan the forest while standing or moving on the ground, which in turn provides a higher level of detail for the under-canopy forest. Consequently, the viewing perspective significantly influences the quantity and quality of data obtained during point cloud acquisition. This implies that the integration of LiDAR point clouds from multiple platforms could contribute to a complementary interpretation of complex forest scenes by reducing occlusion effects and facilitating a more reliable estimation of tree parameters (Calders et al., 2015, 2020).

The use of LiDAR in forests has largely automated the estimation of tree parameters, such as single stem diameter (Oveland et al., 2018; Pitkänen et al., 2019), tree height (Li et al., 2012; Corte et al., 2020; Hyyppä et al., 2020), leaf area index (LAI) and gap fraction (GF) (Stovall et al., 2017). These studies focused on retrieving specific tree parameters using individual LiDAR datasets, which were selected based on the target parameter. However, a complete tree model is more comprehensive and informative; thus, it is desirable. Quantitative structure modelling (QSM) of trees aims to build a comprehensive tree model in which all associated tree parameters can be accurately estimated. The basic idea of QSM is to model different tree segments with geometric primitives, with cylinders being the most commonly used. Geometric primitives are combined to form a complete tree model, involving the basic elements of tree structures, such as stems, branches, and foliage (Raumonen et al., 2013). The aboveground biomass (AGB) of a tree depends mainly on its stems and branches, and tree trunks can be measured directly in the field, although this is difficult for branches (Stovall et al., 2017). Nevertheless, branches can be modeled using the QSM of individual trees with their derived attributes, which include the order, diameter, and length/area/volume of each branch element.

Tree parameters can be further enriched by applying the QSM approach to ground/aerial view-fused LiDAR point clouds. This is because of the complementarity of point clouds acquired from different perspectives, particularly the combination of ground-based and airborne platforms. Challenges in using fusion results from ground-based and airborne LiDAR point clouds for QSM-based tree reconstruction include data redundancy, noisy/outlier points, and misregistration effects because most tree parameters must be determined with centimeter-level accuracy. Therefore, it is desirable to deploy a comprehensive tree model derived from the fusion of ground-based and airborne LiDAR data to overcome such challenges.

In this paper, we present a general framework for QSM-based tree reconstruction from the fusion of ground-based and ULS LiDAR data and assess the retrieved tree parameters that particularly benefit from this fusion. This framework is accomplished in three stages: co-registration of ground-based and ULS LiDAR data, fusion of ground-based and ULS LiDAR data, and investigation of tree parameter retrieval from fused data using QSM.

The main contributions of this study are as follows.

- Identification of co-registration virtual keypoints based on the detection of local density peaks of the clustered canopy.
- Fusion of ground-based and ULS LiDAR point clouds based on the removal of redundancy and noise.
- Investigation of the impact of fused ground/aerial-view LiDAR point clouds on the estimation of tree parameters based on QSM.

The rest of this article is organized as follows: Section 2 describes the literature review on the co-registration of point clouds in forests and the reconstruction of trees from point clouds. Section 3 presents the materials used in this research, including the study area, forest plot descriptions, and data collection. The detailed research methodology of this study is presented in Section 4, and Section 5 describes the experimental design and evaluation scheme. Section 6 presents the results and their interpretations for both point cloud co-registration and tree parameter estimation. Finally, Section 7 presents the conclusions, limitations, and outlook of this research.

2. Related works

The co-registration of point clouds in forested areas is widely reported in the literature. Kelbe et al. (2016) performed marker-free TLS point cloud co-registration by generating view-invariant feature descriptors and applying a voting method to determine the optimal transformation parameter. Paris et al. (2017) completed ALS-TLS point cloud fusion for tree canopy structure assessment by maximizing normalized cross-correlation between a canopy height model from ALS and a corresponding model from TLS using a planar Euclidean transformation. Similarly, Polewski et al. (2016) deployed planimetric and vertical distances between tree locations within the same forest plot to build a similarity function for finding the corresponding trees. Subsequently, two-dimensional (2D) rigid transformation parameters were obtained after a heuristic search over the correspondences. Moreover, Polewski et al. (2019) updated the similarity function and used a simulated annealing algorithm to find a 3D rigid transformation between tree locations from BLS/UAV point clouds. In addition, a triangulated irregular network of tree locations was created to find the corresponding triangles for the fusion of BLS, UAV, and multi-scan TLS point clouds in dawn redwood forest plots (Guan et al., 2019). These methods rely on tree locations to perform co-registration, which is challenging in windy forests and (sub-) tropical forests with high stand density and canopy closureness. Dai et al. (2019) performed co-registration of ALS/TLS point clouds by analyzing common crowns to detect the local maximum of the probability density function. This method utilized coherent point drift to perform a rigid 3D transformation between point clouds. In our study, co-registration was performed using virtual keypoints defined for clusters of forest canopies, without requiring tree segmentation and localization. Furthermore, none of these studies used their co-registration/fusion results for further forest analyses, such as tree parameter estimation, although both ground-based and airborne LiDAR systems have been used for 3D forest mapping (Ye et al., 2019; Calders et al., 2020; Navarro et al., 2020).

In addition, quantitative structural modelling of trees using image-based/LiDAR point clouds has attracted much interest in recent years. Based on the information obtained from point clouds using available LiDAR platforms, several studies for different purposes have been conducted. From a dataset point of view, static TLS is a common platform, because it guarantees high density and low occlusion by integrating multiple scans of the same scene. However, its limitations include multi-scan misregistration, occlusion in single-scan mode, and canopy with sparse point sampling. A wide range of TLS applications in tree reconstruction includes stem curve determination (Wan et al., 2019), branch architecture quantification (Lau et al., 2018), forest inventory parameter derivation (Kalwar et al., 2021), and quantitative structure modeling and biomass estimation (Calders et al., 2015). These studies found that deriving tree heights from TLS data is relatively unreliable. Although TLS can quantify both diameter at breast height (DBH) and tree height, its performance in dense forests still needs to be improved. Hence, the main challenges in applying TLS to forest parameter estimation are associated with occlusion effects and local forest conditions. TLS point clouds have also been used to evaluate the extraction of apple tree branch information from BLS point clouds (Zhang et al., 2020), where only low trees with heights of 3–5 m have been reported to be well modeled by BLS. Ko et al. (2021) reported that BLS estimated the subtropical tree height with lower accuracy than DBH because of the local forest conditions such as

stand density and stem width. Furthermore, the use of point clouds from airborne platforms such as ALS and UAVs has been investigated to determine their suitability for creating tree QSMs. For instance, Hu et al. (2017) has reported tree modelling from ALS data to complement the incomplete point cloud by simulating trunk points based on bounding boxes of tree and ground points. Yao et al. (2012) also reported that only up to 30% of tree stem points in a temperate forest could be captured by airborne waveform LiDAR. Additionally, Liang et al. (2019) found that the stem attributes, including DBH and stem curve, have not yet reached the accuracy level of ground-based LiDAR systems, despite the tree heights with high accuracy provided by ULS. Wang et al. (2019) concluded that ULS-derived AGB is unreliable because of limited access to DBH for ULS and smaller trees in dense boreal forest.

Another study (Navarro et al., 2020) used a UAV point cloud for AGB estimation of mangrove trees; however, the understory and young trees could not be detected by UAV. Moreover, a comparison of the ULS and TLS point clouds was conducted as inputs to *TreeQSM* (Brede et al., 2019). It was concluded that the tree volume was underestimated for dense forest stands from the ULS data due to sparse trunk points. In addition, Shimizu et al. (2022) estimated tree parameters from TLS/UAV-photogrammetry data fusion and reported a remarkable improvement in tree height. Furthermore, Terryn et al. (2022) evaluated the tree parameters derived from the TLS and ULS data against their fusion results which are deemed as a benchmark. They reported that both TLS and ULS-derived parameters were comparable to those of their counterparts from fusion.

Therefore, a combination of point clouds from multiple platforms has not yet been investigated and applied to tree reconstruction based on QSM, although such data integration is expected to enhance forest interpretation and tree parameter estimation. According to the reviewed studies and to the best of our knowledge, the fusion of ground- and aerial-view LiDAR point clouds has not yet been deployed and investigated for QSM based tree parameter retrieval.

3. Materials

3.1. Study site

The study area included seven sample plots in the subtropical forest of Dongtai (120.8263° E, 32.8735° N) in southeastern China. The sample plots contained two tree species: poplar (deciduous) and dawn redwood (coniferous). The sample plots were selected according to GIS-based forest inventory data to cover different forest parameters including tree species, growing stage, and forest structure (e.g. stand density, DBH, and tree height). The ULS sample plots were circles with a 50-m diameter. The sample plots of backpack laser scanner (BLS) and handheld laser scanner (HLS) were squares (30 m × 30 m) to reduce the effect of the alignment errors of the measurements and accuracy degradation during the mobile LiDAR data collection in the final point cloud. The location and distribution of the sample plots within the study area are shown in Fig. 1, and the forest parameters of the sample plots are listed in Table 1. The study area is a planted forest; therefore, the terrain was near-flat without sharp slopes. In addition, the undergrowth structure of the poplar plots (1, 2, 4, and 5) was simple with few and low shrubs. In contrast, there were a large amount of irrigated grass and shrubs in dawn redwood plots (3, 6, and 7).

3.2. Data collection

3.2.1. Field data

Field measurements of DBH, tree height, crown base height (CBH), and crown widths (CWs) in the east-west and north-south directions were taken for 98 individual trees in the seven plots. Fig. 2 shows the distribution of DBH and tree height measurements of the poplar dawn redwood species.

3.2.2. ULS data

The point cloud of the ULS was acquired using the GreenValley UAV

Fig. 1. Study area and location of sample plots. Inset shows the location of Dongtai forest in China. (**a**) Location of the study site in the forest (red rectangle). (**b**) Distribution of the sample plots (green circles) in the study area. (For interpretation of the references to color in this figure legend, the reader is referred to the Web version of this article.)

Table 1
Forest parameters of the sample plots.

Plot	Species	Avg. DBH (cm)	Avg. tree height (m)	Stand density (ha^{-1})	Undergrowth structure
1	Poplar	36.4	31.4	256	Simple with few shrubs
2	Dawn redwood	29.4	17.0	489	Simple with few, low and dense shrubs
3	Dawn redwood	26.7	27.0	233	Complex with large number of irrigated grass and shrubs
4	Poplar	39.7	36.1	222	Simple with a small number of shrubs
5	Dawn redwood	22.8	35.0	578	Simple with few, low and dense shrubs
6	Poplar	36.4	26.9	156	Complex with large number of irrigated grass and shrubs
7	Poplar	22.1	21.3	444	Complex with large number of irrigated grass and shrubs

LiDAR platform. The system consisted of a Velodyne Puck VLP-16 laser sensor, Novatel GNSS receiver, Novatel SPAN-MEMS-IMU, and micro-computer, as shown in Fig. 3a. The flight altitude was 86 m, at a speed of 3.6 m· sec^{-1}. The sensor parameters are listed in Table 2. An example of a ULS point cloud is shown in Fig. 4d.

3.2.3. *Ground-based LiDAR data*

Ground-based LiDAR point clouds were acquired using three platforms: a single-head backpack laser scanner (SBLS), dual-head backpack laser scanner (DBLS), and HLS. The GreenValley BLS system consists of three main parts: a Velodyne Puck VLP-16 scanner, a position and orientation system (POS), and a touch pad for data collection control. The point cloud was generated using the simultaneous localization and mapping (SLAM) technique, which integrates the scanning data and POS information. SBLS data were collected when the single scanner head was mounted horizontally, whereas dual-head mode data were acquired with two scanning heads co-aligned in both horizontal and vertical directions. The ZEB-REVO HLS system was used for point cloud data collection, which consisted of a 2D laser scanner rigidly coupled to an IMU installed on a motor drive. The 3D information was generated by the third dimension provided by the scanning head motion of the motor drive. The 2D scanning data were combined with IMU information for 3D point cloud generation based on SLAM. The typical scan range was 15–20 m outdoors with 270° × 360° fields of view in the vertical and horizontal directions. The system operation in forest mapping is shown in Fig. 3c.

The configuration of the different platforms, as listed in Table 2, influenced the data collection in terms of point density and information details. Fig. 4 shows a poplar-plot example of point clouds collected from the four systems. In Fig. 4a and b, only trunks are acquired in the case of HLS and SBLS. By contrast, the DBLS point cloud provided more information about tree structure at low and relatively high forest levels. It is worth noting that the ground-based dataset is preliminarily aligned to the UAV-LiDAR georeferenced coordinate frame using artificial markers. Coarse alignment resulted in an inaccuracy of greater than 2 m.

4. Methodology

The proposed workflow aimed at performing quantitative structural modelling of trees using ground-based/ULS LiDAR data fusion. This goal was achieved in three leading phases, as illustrated in Fig. 5. Phase I: Markerless co-registration of point clouds; Phase II: point cloud fusion; Phase III: QSM of trees. The detailed steps of these three phases are explained in the following subsections.

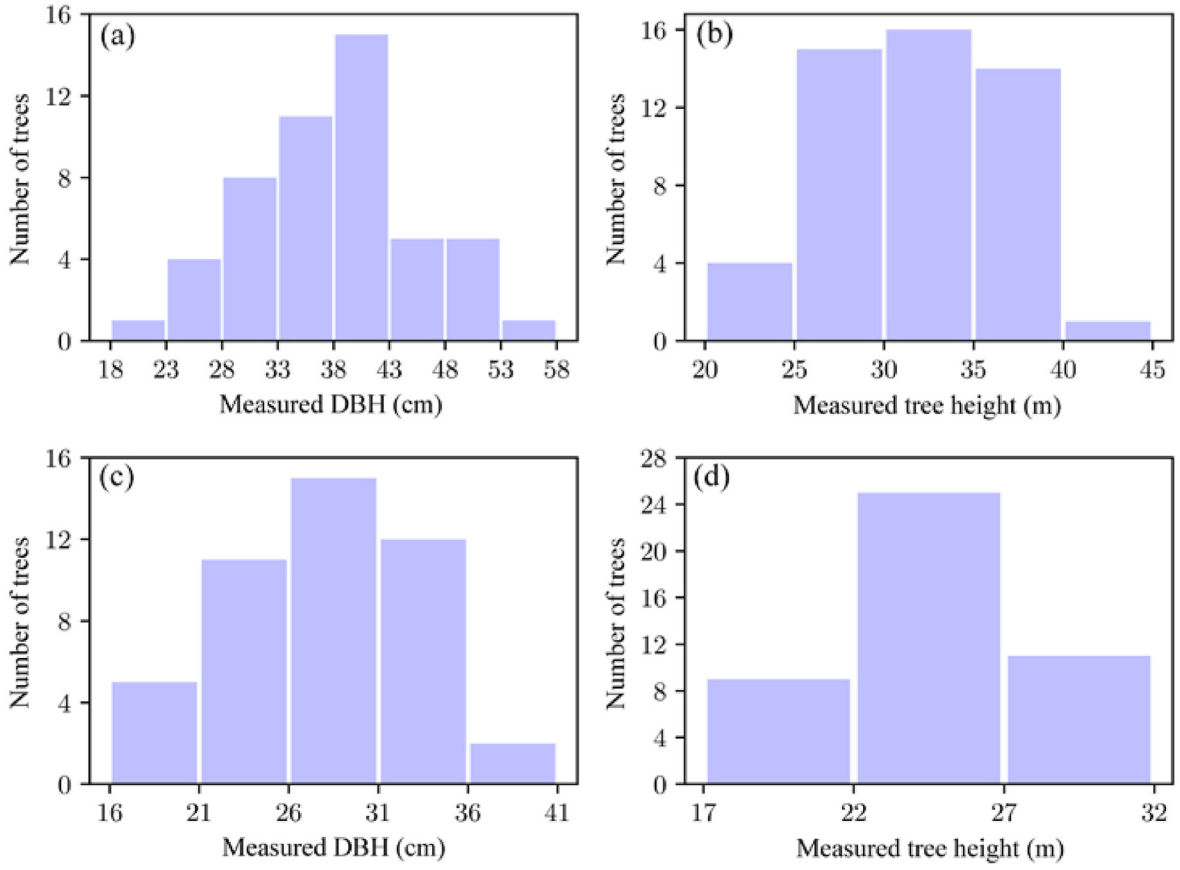

Fig. 2. Histograms of DBH and tree height from field measurements. Top row: poplar species. Bottom row: dawn redwood trees.

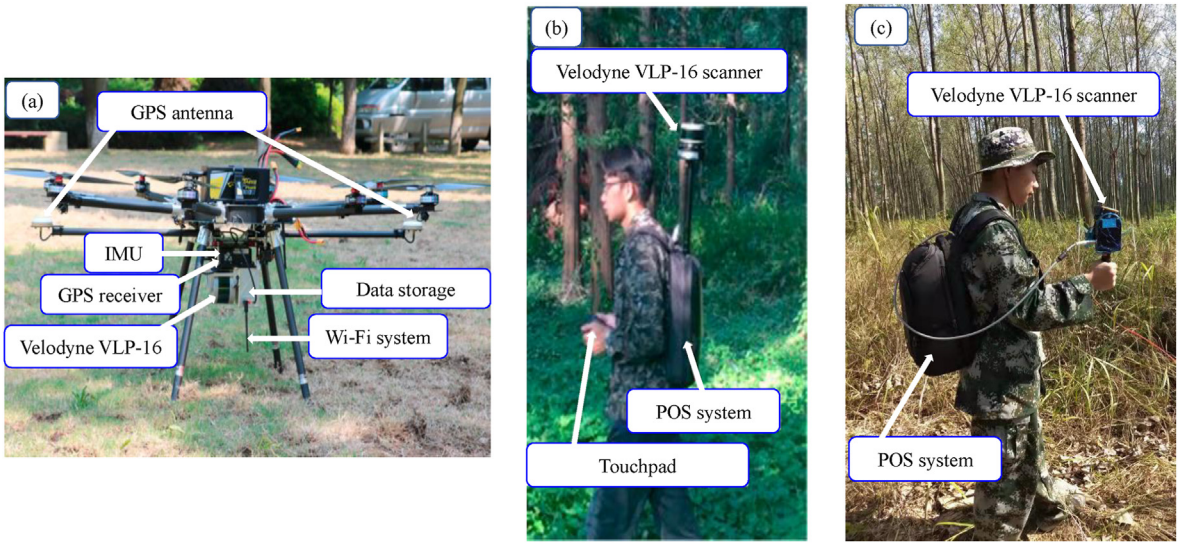

Fig. 3. Different LiDAR systems used for data collection in this study. (**a**) UAV-LiDAR with its main components; (**b**) BLS with its system components; (**c**) main components of HLS.

Table 2
LiDAR sensor parameters for multiple systems.

Parameter	ULS	BLS	HLS
Sensor	Velodyne VLP-16	Velodyne VLP-16	Velodyne VLP-16
Max. range (m)	100	100	15–20
Ranging accuracy (cm)	±3	±3	±(2–3)
Max. footprint (°)	0.1–0.4	0.1–0.4	0.625
Wavelength (nm)	905	905	905
Horizontal FOV (°)	360	360	360
Vertical FOV (°)	30	30	270
Point density (m^{-2})	250 − 300	$(5 - 10) \times 10^3$	$(2 - 4) \times 10^3$
Rotation rate (Hz)	5–20	5–20	100

4.1. Markerless point cloud co-registration

The developed co-registration pipeline, an adaptation of the work of Fekry et al. (2021), was proposed to perform ground/ULS point cloud co-registration. This method developed and implemented an approach to ULS strip alignment in plantation forests by analyzing the topological persistence of point clusters from the forest canopy so as to determine the most stable local maximum.

Depending on the viewing perspective of the LiDAR platform, the local height maxima of the corresponding clusters from the ULS point cloud were nearly identical. Different results were obtained when using data from different perspectives, such as airborne and ground-based LiDAR platforms. The definition of keypoints in Fekry et al. (2021) was replaced by searching for the local density peak of each cluster, rather than topological persistence. The definition of keypoints in the co-registration pipeline allowed the co-registration of ground/ULS point clouds without the need for additional information about the parameters of the tree stand. The definition of the keypoints is described in the following subsection.

4.1.1. Keypoints extraction

Point cloud registration aims to integrate datasets from two or more data-collection platforms, most of which have different perspectives or individual data characteristics. Therefore, defining the appropriate keypoints for co-registration is challenging, particularly when working with forest point clouds with few objects. Moreover, the problem becomes even more complicated in plantation forests, where trees cannot be characterized by species, age, height, stem diameter, etc., because the tree-related parameters are nearly the same at the plot level. Therefore, the scanned canopy was used as a common feature in both the datasets. The canopy was partitioned into point clusters using a hierarchical density-based algorithm (HDBSCAN) (Campello et al., 2013), which requires only one input parameter (MinClusterSize). This algorithm has some special advantages: it learns clusters of arbitrary shapes, marks low-density points as noise, and operates with data of different densities. In this study, clustering was an intermediate step and was not aimed at segmenting individual trees, which meant that a single cluster was not a single crown. The number of clusters from both datasets was not identical, and the ULS point clouds yielded larger ones because the ground-based datasets were subsets of the ULS plots.

A point cloud $\mathbf{PC} \in \mathbb{R}^3$ was partitioned into a set of clusters, $C_k = \{C_1, C_2, C_3, \ldots, C_n\}$, $k \in 1{:}\ n$. We assumed that each single cluster C_k containing any number of points provides a single keypoint. For each point $P_i \in C_k$, two components were computed: the local density ρ_i, which is the number of points within a distance d_c from point i, and its distance δ_i from higher-density points, which is the minimum distance between the point and other higher-density points. Therefore, ρ_i and δ_i depend on the distances d_{ij} between the cluster data points. The two components were compared at high-density points, and the 2D position of the keypoint of C_k was defined as the XY coordinates of the density peak that received the largest δ and highest ρ. A complete 3D keypoint was identified by projecting the extracted local density peak onto the digital elevation model (DEM) of each dataset. This step was required to align the point clouds in the horizontal and vertical directions simultaneously.

$$\rho_i = \sum_j \chi(d_{ij} - d_c), \quad \text{where} \quad \chi(x) = \begin{cases} 1, & \text{if } \chi < 0 \\ 0, & \text{otherwise} \end{cases} \tag{1}$$

$$\delta_i = \min_{j:\rho_j > \rho_i}(d_{ij}), \tag{2}$$

where d_{ij} is the Euclidean distance of a point i from the higher-density points in neighborhood, d_c is the cutoff distance.

A set of keypoints for C_k clusters was generated. Thus, two sets of keypoints were formed: one referred to the point cloud from the ground-based LiDAR (source), whereas the other represented the ULS point cloud (target). The main advantage of this criterion for the extraction of keypoints is that it can mitigate the limitations of tree localization, particularly when integrating point clouds influenced by environmental factors, such as wind, or subject to scene incompleteness acquired from

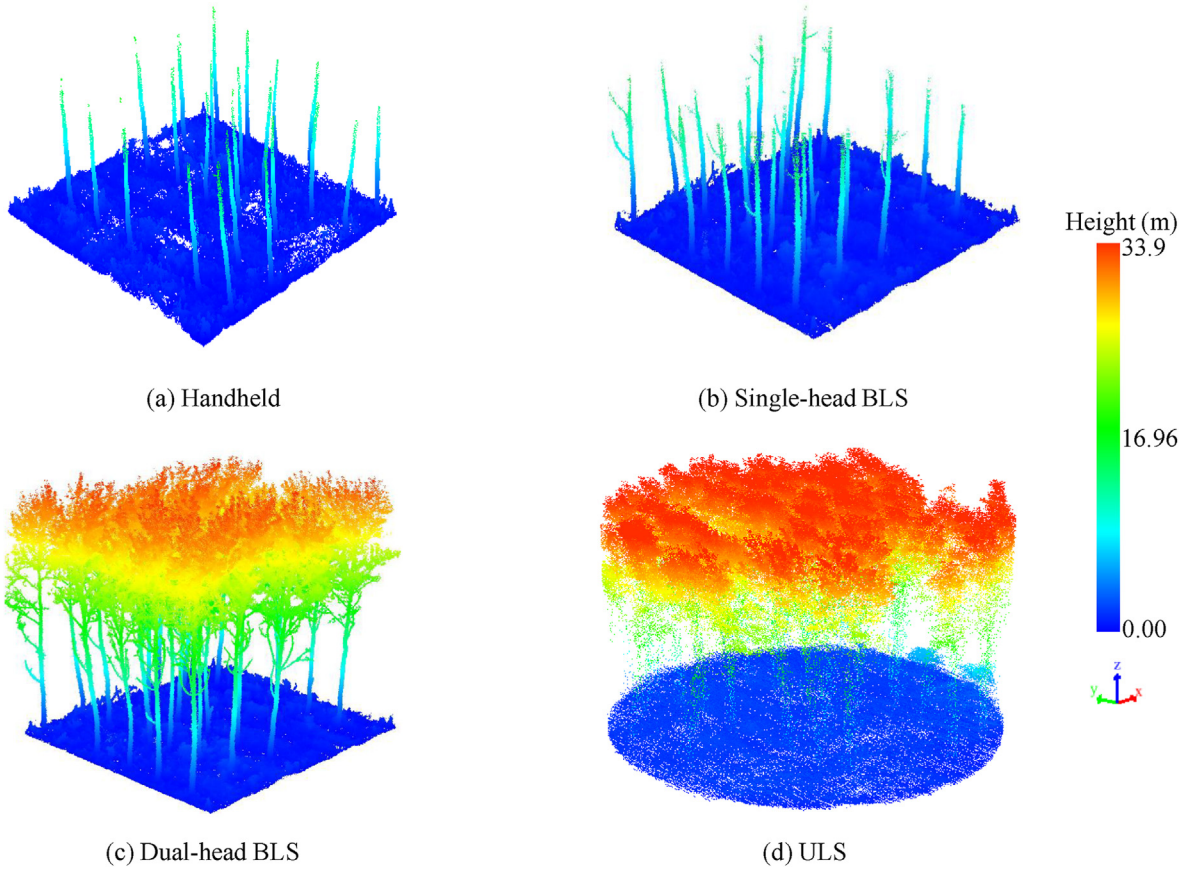

Fig. 4. Point clouds from the four LiDAR platforms for a poplar plot. The influence of the scanning perspective is reflected in the information obtained. (**a**) HLS data; (**b**) single-head BLS data; (**c**) dual-head BLS data; and (**d**) ULS data.

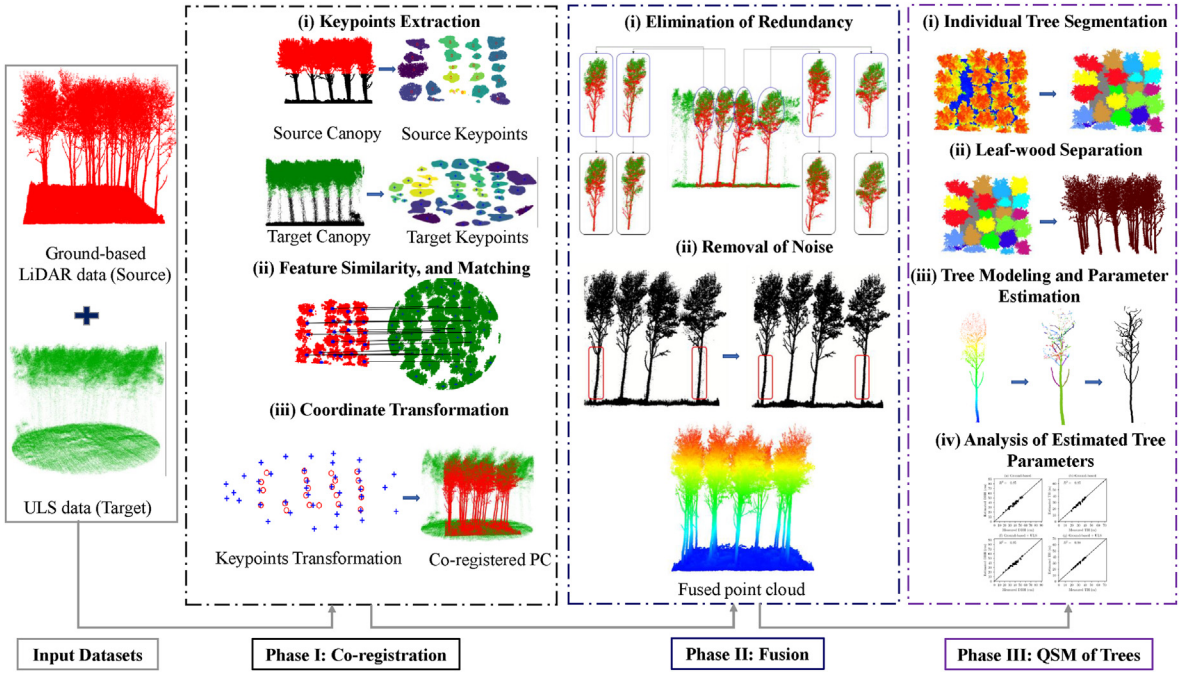

Fig. 5. Research workflow.

different perspectives. For example, Fig. 6 shows two examples of extracted keypoints that are independent of the stem or its center. The full keypoints (red dots) are defined by projecting the extracted peak density points onto a DEM of the point cloud to obtain their heights. Case I in Fig. 6 shows that the stem center and projection of the treetop do not coincide even though the tree is vertical. Case II shows the effect of the

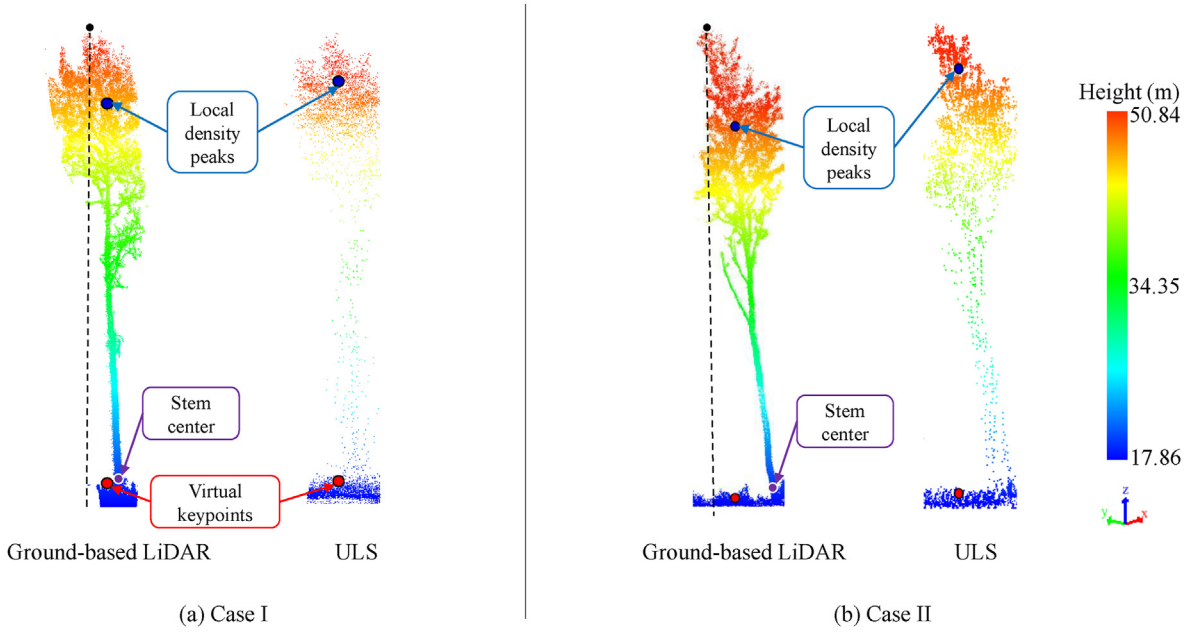

Fig. 6. Extraction of keypoints from the ground-based and ULS datasets. Blue points: extracted points based on density peaks. Red points: full keypoints after projection of the point cloud onto DEM. Dashed lines indicate the non-coincidence between the treetop and stem center. Case I: the stem center and projection of the treetop are not identical even though the tree is vertical. Case II: effect of the tree being skewed owing to its growth or environmental factors. (For interpretation of the references to color in this figure legend, the reader is referred to the Web version of this article.)

tree being skewed owing to its growth or environmental factors, resulting in the same situation as in Case I.

4.1.2. Feature matching and transformation

Following the extraction of keypoints, the feature matching and transformation procedure of Fekry et al. (2021) was applied to co-register the ground-based and ULS point clouds. Feature descriptors were formed based on the distance and bearing angle of each point to the centroid of the point set. Subsequently, one-to-one correspondence was determined by graph matching. Finally, three-dimensional rigid-body transformation parameters with six DoF (three rotations R_Z, R_Y, R_X, and three translations T_X, T_Y, T_Z) between the source $\boldsymbol{X}_S$ and target $\boldsymbol{X}_T$ keypoints sets were calculated, as shown in Equation (3). Fig. 7 shows the keypoints from the ground-based point cloud and the ULS before and after co-registration.

$$\boldsymbol{X}_T = \boldsymbol{R} \times \boldsymbol{X}_S + \boldsymbol{T}_{XY\,Z}, \tag{3}$$

where $\boldsymbol{R}$ is the rotation matrix, and $\boldsymbol{T}_{XYZ}$ is the translation vector in X, Y, and Z, respectively.

There were still some discrepancies between the co-registered point clouds, which posed a challenge for tree parameter estimation because they should be computed at the centimeter level. Therefore, the distance between point cloud pairs should to be further minimized. The most common fine-registration algorithm is the iterative closest point (ICP), which finds a rigid transformation to align the source point cloud with the target cloud. Fig. 8 shows an example of the effect of the ICP refinement on the final co-registration results. The focus is on overlapping crowns, where the green points belong to the ULS cloud, and the ground-based dataset is shown in red. It can be observed that the top-level benefits strongly from ICP, whereas the lower-levels contain fewer points from the ULS.

4.2. Point cloud fusion

The main goal of fusion is to integrate two or more registered point clouds to create a new dataset that leverages each one. The level of detail (LoD) of ground based and ULS LiDAR point clouds is different. For example, the ULS point density varied spatially and was relatively lower than the point cloud density of the ground-based LiDAR platforms. However, the ULS point cloud enabled terrain reconstruction and surface modelling despite the lack of points under the canopy and near the ground. By contrast, the ground-based dataset was derived from two

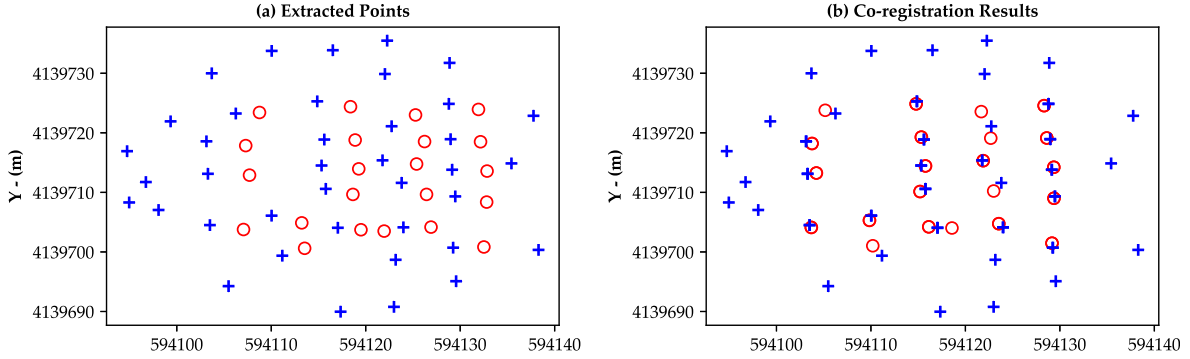

Fig. 7. Transformation of keypoints by permutations. Red circles: source keypoints (ground-based LiDAR). Blue crosses: target keypoints (ULS dataset). (**a**) Before co-registration, and (**b**) Co-registered keypoints. (For interpretation of the references to color in this figure legend, the reader is referred to the Web version of this article.)

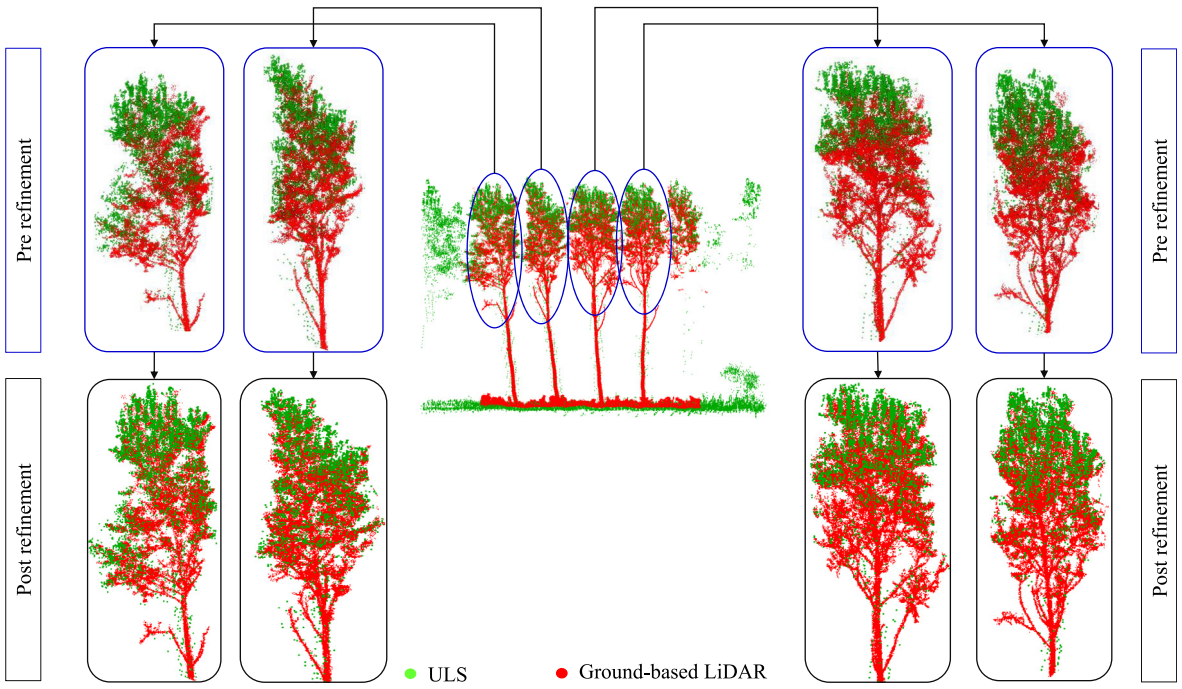

Fig. 8. Profile along a poplar plot showing the refinement of co-registration results according to ICP. An example result shows the minimization of discrepancies between ground-based (red) and ULS point clouds (green). (For interpretation of the references to color in this figure legend, the reader is referred to the Web version of this article.)

mobile LiDAR devices that provided a high point density at lower levels. This resulted in a detailed representation of the tree trunks and branches, whereas the point density was limited to higher levels of the tree canopy. Fusion targets common objects that are mostly exclusively present in the upper forest layers in the case of ground-based and ULS LiDAR data fusion. This feature difference in the point cloud may lead to conflicts as some points are redundant, whereas others are considered as noise or outliers. Fig. 9 shows an example of co-registered point clouds of a poplar tree, where scattered points surrounding its stem are noise, and its top contains complementary points. The redundant points increase the computational cost by posing potential conflicts in the structure, whereas noisy points can severely affect tree modelling, particularly cylinder fitting. Therefore, noisy points were prioritized during the removal process. The detailed steps for removing noise and redundancy are as follows:

4.2.1. Elimination of redundancy

The co-registered point clouds included data from two perspectives. Therefore, there were a large number of undesirable points in the overlapping areas, which were classified as noise and redundant. The noisy points are mainly represented by the scattered points around the stems, as shown in Fig. 11a, most of which emanate from the ULS point cloud. However, the redundant points were captured by both datasets and eliminating them did not affect the quality of the point cloud. Redundant points were first detected and removed to reduce the computational cost and alleviate potential conflicts in the structure.

The scattered point cloud **PC** contained a set of points in $\mathbb{R}^3$. It was partitioned into small cubes of side length l. For each point p_i, the distances to all points within the cube were computed. All points whose distances to p_i were smaller than a threshold ε were considered redundant and were therefore eliminated. In the case of ground-based and airborne LiDAR data fusion, the crowns have the most overlap, and redundant points are nearly always present. Thus, the redundancy elimination was performed on the fused point cloud to preserve only the most important information. Fig. 10 shows the results of redundancy removal from the fused point cloud, with the higher tree levels magnified to show how they appear after redundancy removal. Redundant points come from ULS dataset with sparse points on tree trunks and branches. Under-canopy levels still contain scattered points around the trunks and branches, which are problematic for the modelling algorithm. Therefore, these points were considered noise and removed based on statistical filtering of the point cloud.

4.2.2. Removal of noise

A statistical method (Ning et al., 2018) was used to remove noisy points by computing the distribution of distances between points and their neighbors in the dataset. Considering a Gaussian distribution with its mean and standard deviation, the neighbor points with mean distances outside the interval defined by the mean and standard deviation of the global distances were considered as noise and were therefore removed from the dataset.

The scattered point cloud **PC** contains a set of points in $\mathbb{R}^3$. For each point $p_i \in$ **PC**, the local neighborhood p^{nbr} within a fixed radius ν is determined for each point $p_i \in$ **PC**. The mean distance D_i from p_i to its neighbors k in p^{nbr} is computed as follows:

$$\overline{D_i} = \frac{1}{k}\sum_{j=1}^{k} \mathbf{ED}\left(p_i,\ p_j^{nbr}\right), \tag{4}$$

where **ED** is the Euclidean distance between p_i and its neighbor $j \in p^{nbr}$. The Gaussian distribution GD(p_i) for p^{nbr} in p_i is represented as follows:

$$\mathrm{GD}(p_i) = \frac{1}{k}\sum_{p_j^{nbr} \in p^{nbr}} \exp\frac{-\mathbf{ED}\left(p_i,\ p_j^{nbr}\right)}{\overline{D_i}} \tag{5}$$

The probability of considering p_i as a noisy point is computed using GD(p_i), as expressed in Equation (6), where σ is the probability threshold.

$$Pr(p_i) = 1 - \mathrm{GD}(p_i) \quad \text{where} \quad p_i \quad \text{is} \quad \begin{cases} \text{noise}, & \text{if } Pr(p_i) > \sigma \\ \text{retained}, & \text{otherwise} \end{cases} \tag{6}$$

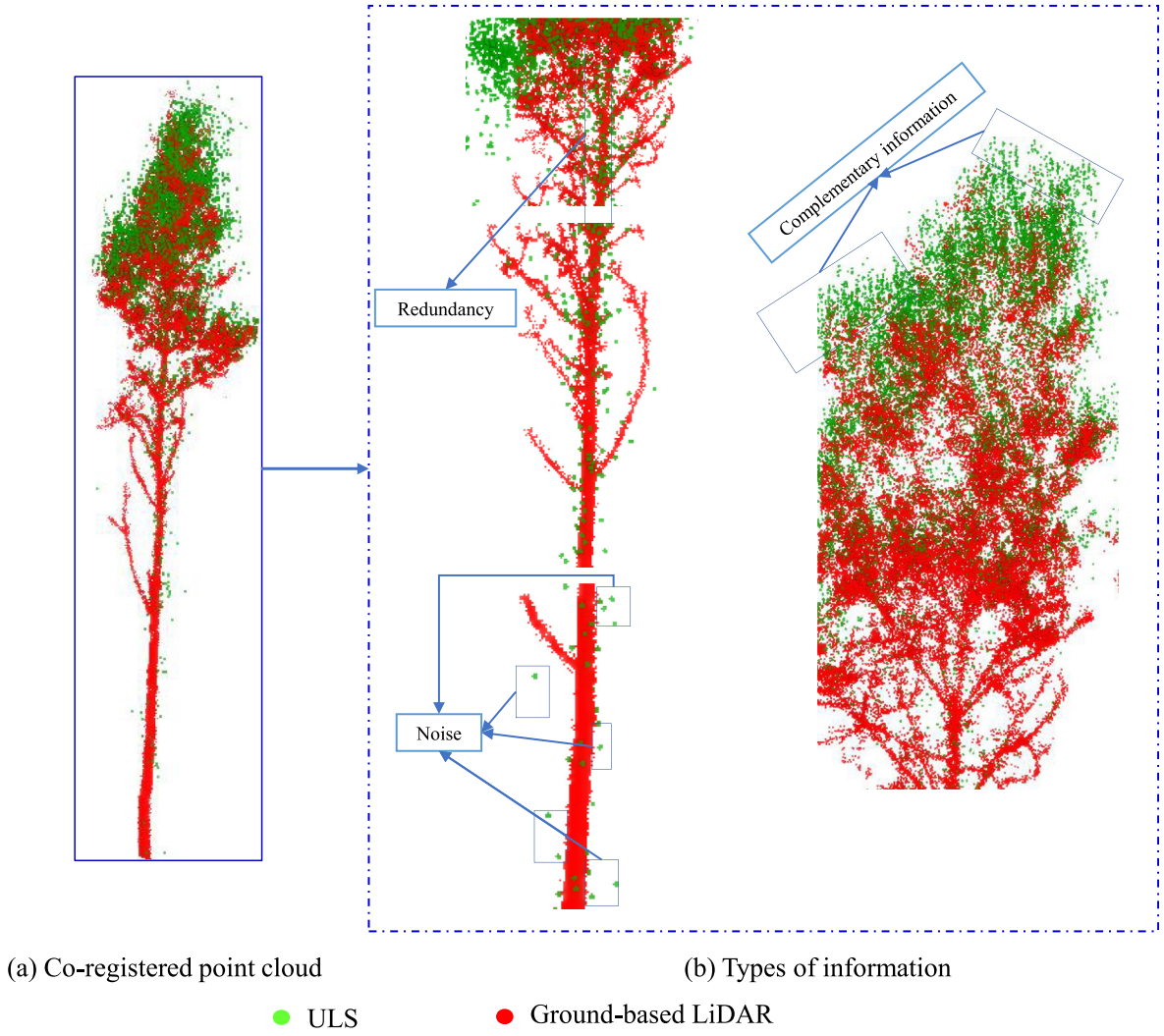

Fig. 9. Co-registered point clouds with the different types of conflict points. (**a**) Co-registered point cloud of a tree, and (**b**) different types of points within overlapping regions. Redundant points from ULS (green color) existed particularly at the high-tree levels on the trunk and canopy. Noisy points were scattered around the stem and branches at the low-tree levels. (For interpretation of the references to color in this figure legend, the reader is referred to the Web version of this article.)

Noisy points are shown in the vicinity of the stems from the ULS point cloud, as highlighted by the red rectangles in Fig. 11. Moreover, redundant points are mainly found in the crown region, which has the largest overlap between the two datasets.

4.3. Tree modelling

4.3.1. Individual tree segmentation

Tree segmentation is essential for reconstruction. If it is performed accurately, the structural attributes of the tree can be estimated, including the DBH, height, basal area, and wood volume. Various tree segmentation approaches have been developed. In this study, individual trees were accurately segmented in three steps (Tao et al., 2015): normalization of the point cloud, stem detection and estimation of DBH, and segmentation of the crown. A DEM was generated from the point cloud using ordinary kriging (Guo et al., 2010), and the point cloud was normalized by subtracting the heights of the DEM from the heights of the point cloud.

4.3.2. Leaf-wood separation

Reconstruction of trees from the point cloud mainly focused on the woody part because the leaves and foliage did not have a uniform distribution, which might affect the final modeling results. The classification of forest point clouds into woody and foliage clouds has been studied from different perspectives. Based on the classification features, the developed methods can be categorized as geometric (Wang et al., 2018; Moorthy et al., 2020), radiometric (Béland et al., 2013) or both (Xu et al., 2021). In this study, the method of Moorthy et al. (2020) was adopted for classification purpose. The main advantage of this classification method is that it can function with point clouds of varying densities by exploiting multi-scale features.

The algorithm was employed to classify forest point clouds by combining the geometric features of the normalized eigenvalues and the zenith angle of the eigenvectors of each point at multiple spatial scales. The eigenvalues λ_0, λ_1, and λ_2 represent the distribution of points within the neighborhood, where the local neighborhood of each point is defined by setting a sphere of radius $\mu = \{\mu_1, \mu_2, \mu_3, \ldots, \mu_n\}$. The eigenvectors and eigenvalues were obtained by first computing the covariance matrix of the local neighborhood of each point following the procedure in Belton et al. (2013) according to Equation (7).

$$\Sigma_{3\times3} = \frac{1}{n}\cdot\sum_{i=1}^{n}(p_i - p)(p_i - p)^T, \tag{7}$$

where p_i is the i^{th} point of n points in the neighborhood, and p is the mean of the neighborhood coordinates. Then, the eigenvalues were obtained by decomposing $\Sigma_{3\times3}$ using Equation (8). The eigenvalues were

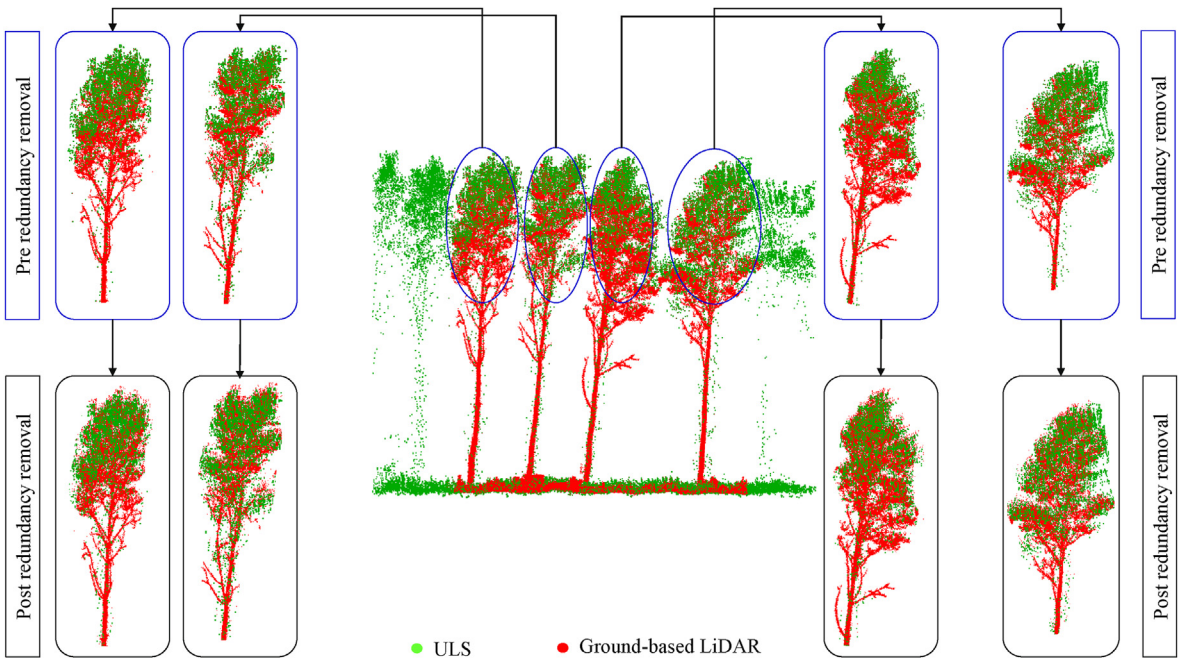

Fig. 10. Profile along a poplar plot showing the removal of redundant points. An example result shows the removal of duplicate points in the co-registered point clouds. The ground based and ULS datasets are shown in red and green, respectively. (For interpretation of the references to color in this figure legend, the reader is referred to the Web version of this article.)

normalized to the range [0, 1] by dividing each eigenvalue by the sum of λ_0, λ_1 and λ_2.

$$\Sigma_{3\times3} = \sum_{i=0}^{2} \lambda_i . e_i . e_i^T \tag{8}$$

where λ_i is the eigenvalue in a direction i within the neighborhood, and e_i is the unit vector in direction i. On a spatial scale $\mu \in \{\mu_1, \mu_2, \mu_3, \ldots, \mu_n\}$, let the normalized eigenvalues at μ be λ_1, λ_2, λ_3 such that $\lambda_1 > \lambda_2 > \lambda_3$ and their corresponding zenith angles of the eigenvectors are θ_1, θ_2, and θ_3. The computation of such features at each point was used to capture the distributions of different tree segments such as the trunk, branches, and leaves on a local spatial scale. The first eigenvalue λ_1 of the trunk and branches was greater than λ_2 and λ_3, and the zenith angle of the trunk was always near 0° or 180°, whereas this was not the case for leaves and branches. Therefore, woody and leafy points can be distinguished based on the differences in their distributions. An example of this result is shown in Fig. 12, where the poplar species are shown in the top row and the dawn redwood species in the bottom row. The left column shows the raw point cloud, and the right column shows only the woody parts of the point clouds of the two example plots.

4.3.3. Tree parameter estimation

A variety of algorithms have been used to perform tree modeling based on QSM, including *TreeQSM* (Raumonen et al., 2013), *SimpleTree* (Hackenberg et al., 2015), and *PypeTree* (Delagrange et al., 2014). *TreeQSM* is mostly used for tree reconstruction and the experiments involving destructive methods show that it can achieve high accuracy in parameter estimation. Although the model should be continuously improved in terms of parameter optimization and visualization, the geometric topology of the tree branches is an impediment. The *SimpleTree* algorithm is relatively complicated because it requires the branch diameter as the input and does not construct a branch cylinder to recover its geometry. By contrast, *PypeTree* only provides a general description of the topological structure of a tree without reconstructing the branches.

In this study, the algorithm *TreeQSM* was used to reconstruct the trees based on QSM. The algorithm covered the tree point cloud with small contiguous patches and used a building-brick approach to create a tree surface from these patches. Cylinders of different sizes were used to approximate the trunks and branches. Small cylindrical patches were used to reconstruct the tree segments in the two main phases. In the first phase, the coarse structure of the tree was identified using large patches of constant size with a radius (Patch Diameter1) that crossed the tree. In the second phase, a fine cover set ranging from Patch Diameter2 (min) to Patch Diameter2 (max) was used to obtain branches. The individual branches were then reconstructed using the least squares of the connected cylinders.

One of the important considerations in *TreeQSM* is the Patch Diameter2 (min) setting, as it determines the extent to which the smallest branch element can be reconstructed, and thus the level of detail recovered from the data. Finally, the tree segments were geometrically reconstructed: the trunk was reconstructed from the base of the tree to its top using the neighborhood of the cover sets that had been enlarged to form the trunks. For more information on *TreeQSM*, see Calders et al. (2015), Gonzalez de Tanago et al. (2018), and Raumonen et al. (2013). An example of tree modeling based on *TreeQSM* is shown in Fig. 13.

5. Experimental design

5.1. Parameter setup

The main parameters utilized for point cloud co-registration were the minimum number of points required to form a cluster in HDBSCAN, which was derived from the point cloud density, and the distance threshold, D_{thr} = 1 m. The inputs of the algorithm *TreeQSM* were PatchDim1 = [0.06, 0.09], PatchDim2Min = [0.0364, 0.0674], and PatchDim2Max = [0.0485, 0.09]. The DEM was created at a resolution of 0.5 m.

5.2. Evaluation scheme

5.2.1. Co-registration

The co-registration results were evaluated by calculating the distance residuals between the matched keypoints from the ground-based and the ULS point clouds. Accordingly, the Euclidean distances between the

Fig. 11. Profiles along the point clouds showing the effects of removal of noise and redundant points from the ground-based/ULS fusion results. (**a**) and (**b**) one case of poplar plot, (**c**) and (**d**) one case from a dawn redwood plot.

matched keypoints were calculated after the co-registration. Let $\boldsymbol{x}_i$ and $\boldsymbol{x}_j$ be the 3D coordinates of the matched keypoint pair, $i \in \boldsymbol{X}_S$ source keypoints and $j \in \boldsymbol{X}_T$ target keypoints, respectively. Let the Euclidean distance between the two points $ED_{ij} = \|\boldsymbol{x}_i - \boldsymbol{x}_j\|$. The smaller the ED_{ij}, the higher the accuracy of co-registration. Additionally, the matching percentage was calculated for all plots as $\frac{\text{N}^\text{o}\text{ of matched points in thr}}{\min(\text{source}_{\text{points}},\ \text{target}_{\text{points}})}$.

5.2.2. Tree parameter estimation

The tree parameters obtained by modeling the corresponding individual trees (poplar and dawn redwood species) based on the ground-based dataset and ground-based/ULS LiDAR data fusion were compared to their corresponding field measurements. DBH, tree height, tree volume, crown area, and crown volume were evaluated based on the reference field measurements. The evaluation was performed in terms of the coefficient of determination, R^2, root-mean-square error, RMSE, and relative root-mean-square error, rRMSE.

Because field measurements were not performed directly for tree volume (V), crown area (CA), and crown volume (CV), they were calculated based on the field measurements of DBH, tree height, CBH, and CWs. In this study, the V of poplar and dawn redwood tree species was calculated using models from Gao et al. (2021) because they were developed for similar forest types and tree species. The standard volume was computed based on the correlation between tree height and DBH as stated in Equation (9).

$$V = \begin{cases} \dfrac{1.501 \times K \times D^{1.901}}{2.724 \times H^{2.724}} \times H^{1.854}, & \text{Poplar tree species} \\ \dfrac{0.598 \times K \times D^{1.9}}{2.417 \times H^{1.279}} \times H^{2.417}, & \text{Dawn redwood tree species,} \end{cases} \tag{9}$$

where H and D represent the tree height and DBH, respectively, while K is a constant $\approx \frac{1}{40000}$. Moreover, the field measurements of CBH and CWs were used to generate the ground truth for the CA and CV based on the geometric simulation. The CA was calculated as the oval area of the crown projection $\frac{\pi ab}{4}$, where a and b are the measured crown widths. Additionally, the ground truth of the crown volume CV was computed as the volume of a paraboloid based on the average crown diameter $C_D = \frac{a+b}{2}$ and crown length $C_L = H$ – CBH as $\text{CV} = \pi \frac{C_D^2 C_L}{8}$.

6. Results and discussion

6.1. Markerless co-registration of point clouds

Ground-based LiDAR point clouds were successfully co-registered with ULS point clouds in all sample plots. The distance residuals at the matched keypoints from ground-based and ULS data of each plot are calculated according to the criteria in Section 5.2.1. Fig. 14 shows the

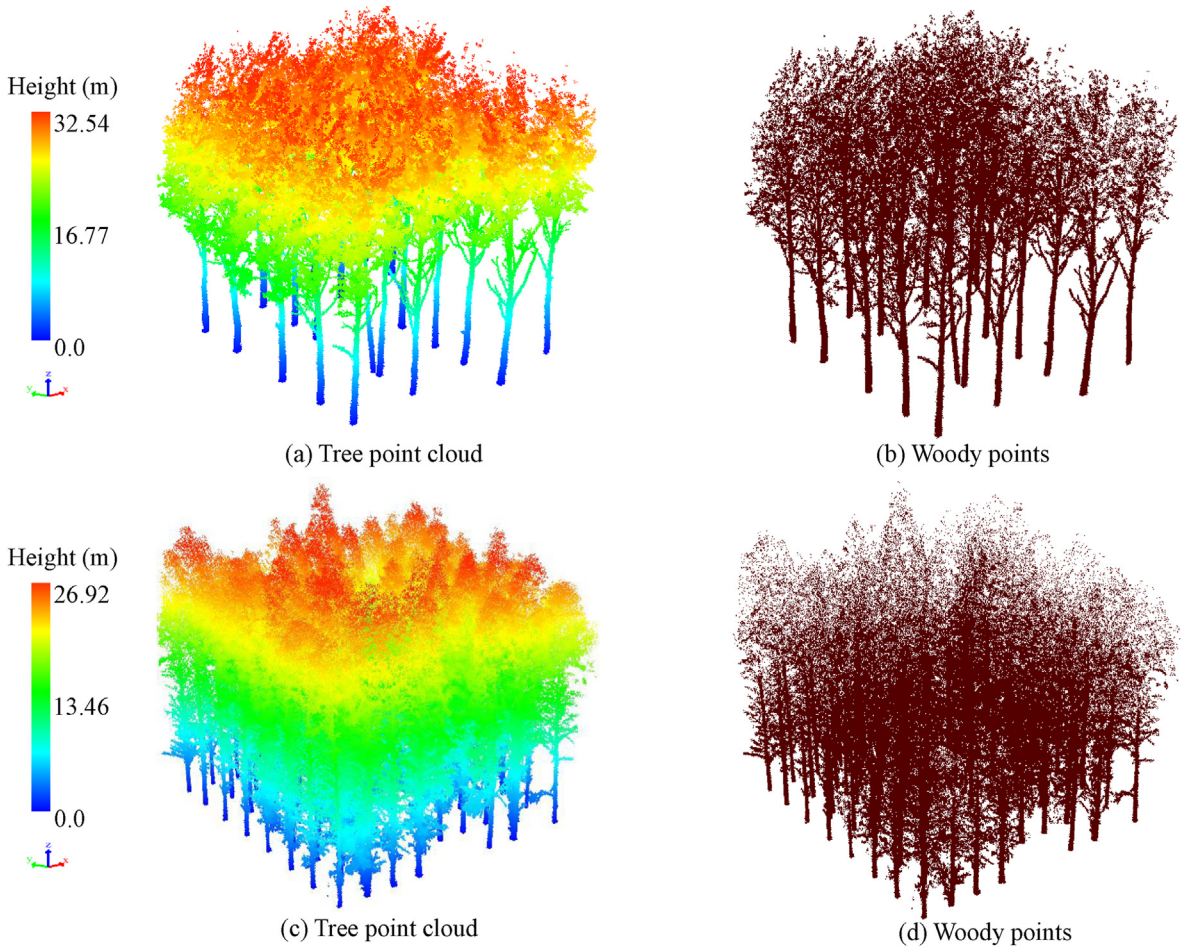

Fig. 12. Classification of point cloud into wood and leaves. (**a**) and (**b**) one case of poplar plot, (**c**) and (**d**) one case of dawn redwood plot. Point clouds are colored with respect to height and the woody parts are represented in brown. (For interpretation of the references to color in this figure legend, the reader is referred to the Web version of this article.)

distribution of these distance residuals of each plot, where the red lines represent the medians of the distance residuals in each plot. The residuals in each plot were divided into four parts, such that each part contained 25% of the residuals, and the rectangular part represented the interquartile range and contained 50% of the data. The interquartile ranges of the poplar plots (1, 4, and 7) varied from 30 to 60 cm, except for plot 6, which ranged from 30 to 50 cm. However, the dawn redwood plots (2 and 3) had larger interquartile ranges of 40–70 cm, with the exception of plot 5, which ranged from 40 to 55 cm.

In general, the lower mean distance residuals of poplar plots 1, 4, 6, and 7 were lower than those of dawn redwood plots 2, 3, and 5 . According to the plot-level forest parameters listed in Table 1, poplar plots 1 and 4 have relatively high stand densities and average tree heights, thus, their mean distance residuals are comparable (the difference is 2.1 cm). By contrast, the stand density of dawn redwood plot 3 was approximately half that of plot 2, whereas the difference between their mean distance residuals was 1.9 cm. Although the stand densities of poplar plots 1 and 4 were relatively comparable to those of dawn redwood plot 3, the differences in the mean distance residuals between them were 7.6 and 9.7 cm, respectively. Moreover, the stand density of dawn redwood plot 2 and poplar plot 7 was 489 and 444 ha^{-1}, respectively, and the mean tree height of plot 7 was greater than that of plot 2. The difference in mean residuals between the two plots was 10.9 cm. Thus, the method performed well on different stand properties with comparable co-registration accuracy.

Fig. 15 shows an example of point cloud co-registration for two cases: deciduous (top row) and dawn redwood plots (bottom row). It can be observed that the horizontal and vertical discrepancies between the point cloud pairs are very low. Moreover, the trunks are fairly visible in the ground-based dataset (red), whereas the treetops are considerably distinct and dense in the ULS dataset (green). It is expected that the fusion results will benefit from the complementarity of datasets acquired from platforms with different perspectives.

In order to investigate the effect of the differences of the point density between ground-based data and ULS point cloud, the matching rate was compared in the case of original and downsampled ground-based data. It was found that the matching rate was improved by a range of 8%–15% at all plots after downsampling the ground-based LiDAR data. Thus, proper downsampling is required as a pre-processing step for the higher density point cloud. In addition, the co-registration results were compared to those of two previous studies (Guan et al., 2019; Polewski et al., 2019) which relied on tree locations as the keypoints. Guan et al. (2019) retrieved the correspondence from the matching of TIN formed by tree locations to co-register BLS, UAV-LiDAR, and multi-scan TLS for two sites of dawn redwood tree species. The reported distance residuals after coarse registration were 84 and 93 cm for sites I and II, respectively. Our study achieved a maximum of 75 cm for all distance residuals in the dawn redwood plots, as shown in Fig. 14. Polewski et al. (2019) co-registered BLS and UAV-LiDAR data of seven sample plots (i.e. four deciduous plots and three dawn redwood plots) from a subtropical forest based on the distances between the tree locations and obtained the rigid 3D transformation by simulated annealing optimization. The recorded matching percentages of deciduous plots ranged from 36% to 48%, and the average residuals between the matched points varied from 62 to 67 cm. In our

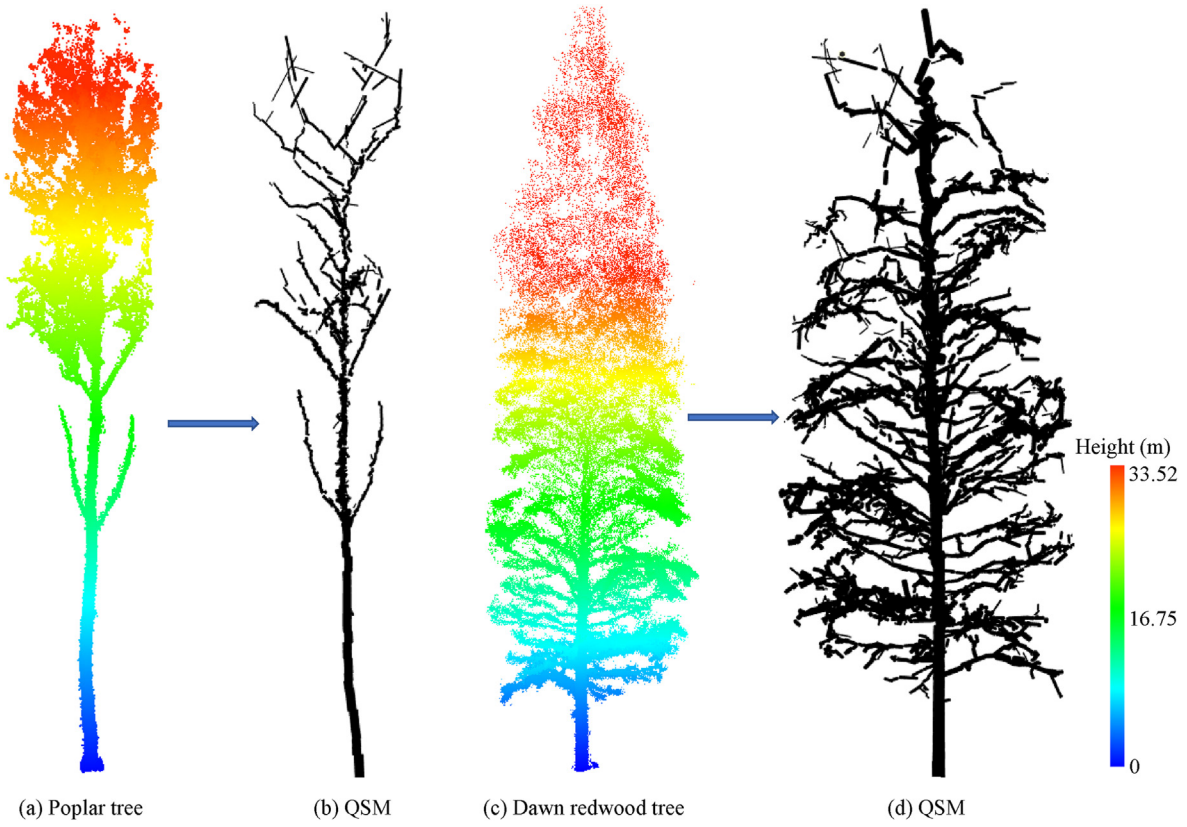

Fig. 13. Tree modeling based on the *TreeQSM* algorithm. (**a**) and (**b**) poplar tree. (**c**) and (**d**) dawn redwood tree.

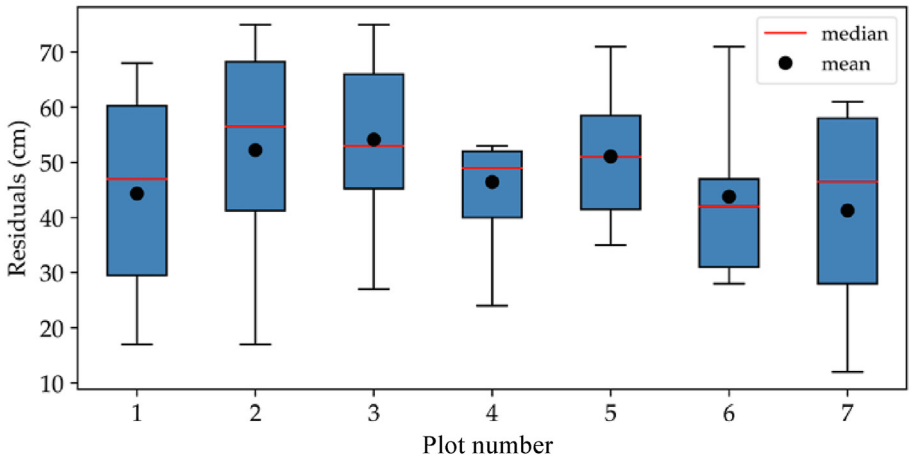

Fig. 14. Distribution of distance residuals at the matched keypoints of each plot. Red lines: median of residuals. Filled circles: mean of residuals. (For interpretation of the references to color in this figure legend, the reader is referred to the Web version of this article.)

study, the range of matching percentages achieved at the deciduous plots was 37%–73% and the range of mean distance residuals was 41.3–46.5 cm. It is shown that the co-registration of deciduous plots is improved in terms of both matching rate and accuracy, implying that virtual key-points could outperform tree locations. Both quantities are also compared for the dawn redwood plots and the matching rate of dawn redwood plots of the results obtained in our study ranged from 39% to 56% and the distance residuals ranged from 51.1 to 54.1 cm which did not improve the co-registration compared to the baseline method that yielded matching rates ranging from 46% to 72% and average distance residuals ranging from 27 to 36 cm. This can be attributed to the existence of distinct treetop shapes in dawn redwood species.

6.2. *Tree parameter estimation*

The tree parameters were estimated by modeling the corresponding trees from the ground-based LiDAR and fused point clouds based on *TreeQSM*. The main advantages of using the *TreeQSM* algorithm in tree modeling are that it made no assumptions about the different tree species or architectures, and the fast retrieval of all tree parameters including the tree volume based on trunk and branches, trunk length and its taper function, the bifurcation frequency, topology, and branching angles. Other tree parameter estimation methods focused on single parameters such as DBH, tree height or crown attributes while no information about the branches or bifurcation frequency. The computed evaluation metrics

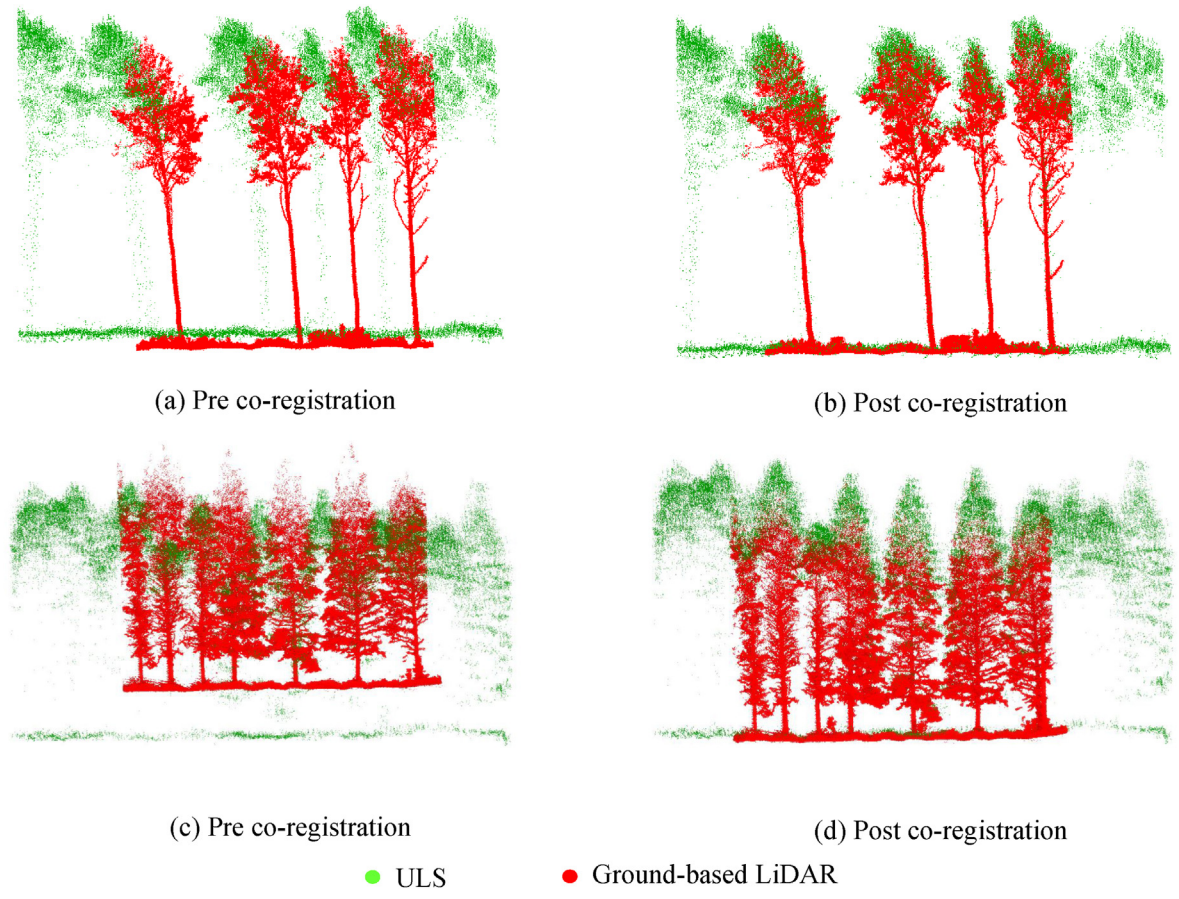

Fig. 15. Profiles along poplar (top row) and dawn redwood (bottom row) plots, with the right column showing the results of point cloud co-registration. Source point cloud: ground-based dataset (red color). Target point cloud: ULS dataset (green color). (For interpretation of the references to color in this figure legend, the reader is referred to the Web version of this article.)

are summarized in Table 3. Fig. 16 and Fig. 17 show the correlation between the estimated tree parameters from ground-based and fused LiDAR point clouds with respect to field data for poplar and dawn redwood trees, respectively. Generally, it was found that fusion-derived *H*, *V*, and CV were strongly correlated with field data based on R^2 compared to ground-based LiDAR only. Additionally, the *r*RMSE for the aforementioned parameters were enhanced (H = 9.01%, V = 5.28%, CV = 18.61%). Such improvements can interpret the more precise parameter estimation from fusion compared with the ground-based dataset. By contrast, fusion-derived DBH and CA were not significantly improved in terms of *r*RMSE (DBH: −0.5%, CA: 2.01%) compared with ground-based data. It is worth mentioning that fusion-derived DBH was not improved compared to ground-based DBH because the stems could not be sampled from the ULS data. The fusion-derived CA did not report a strong improvement because the crown base was independent of the clumped canopy.

Based on the plot parameters, it is worth noting that the stand density of dawn redwood plots was relatively higher than that of the poplar plots. Therefore, the clumped canopy of dawn redwood plots would weaken ground-based LiDAR penetration to higher tree levels and vice versa for ULS. In view of this, the tree parameter estimation of poplar plots gained less benefit than that of dawn redwood plots. For instance, the *r*RMSE of *H* and CV was improved by up to 4.87% and 1.63%, respectively, compared to 9.01% and 18.61% for dawn redwood species. By contrast, the *r*RMSE improvement in *V* from poplar trees was slightly better than that of dawn redwood trees (by 0.41%), which could be attributed to the thicker poplar trees than dawn redwood. Higher tree levels were mainly sensed by the ULS. Accordingly, thinner trunks/branches would not be well sampled, and thus could not be modeled by cylinder fitting through *TreeQSM*. The *r*RMSE of fusion-derived CA was not significantly improved for either tree species (dawn redwood: 0.75%, poplar: 2.01%) because the crown base is accessible from the bottom levels by ground-based LiDAR independent of canopy clump. In addition, the CV of poplar trees benefited less from fusion (1.61%) than dawn redwood

Table 3
Evaluation metrics of estimated parameters based on field measurements.

	Dawn redwood species						Poplar species					
	R^2		RMSE		*r*RMSE (%)		R^2		RMSE		*r*RMSE (%)	
	Ground	Fused	Ground	Fused	Ground	Fused	Ground	Fused	Ground	Fused	Ground	Fused
DBH	0.93	0.92	1.43 cm	1.55 cm	5.27	5.77	0.95	0.95	1.75 cm	1.82 cm	4.67	4.84
H	0.83	0.96	3.25 m	1.10 m	13.59	4.58	0.95	0.98	2.72 m	1.19 m	8.63	3.76
V	0.82	0.88	0.029 m^3	0.023 m^3	23.45	19.07	0.88	0.92	0.064 m^3	0.049 m^3	22.34	17.06
CA	0.88	0.90	6.89 m^2	6.39 m^2	10.43	9.68	0.84	0.86	4.39 m^2	3.91 m^2	18.56	16.55
CV	0.80	0.89	14.46 m^3	6.55 m^3	34.03	15.42	0.95	0.96	20.11 m^3	17.70 m^3	13.6	11.97

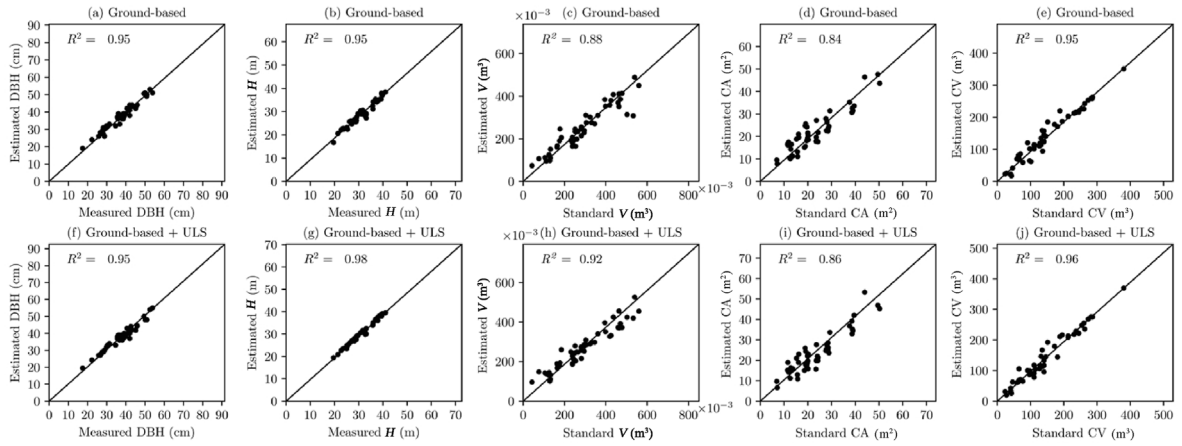

Fig. 16. Scatterplots of estimated tree parameters and field measurements of poplar species. Top row: ground-based LiDAR data. Bottom row: fused point cloud.

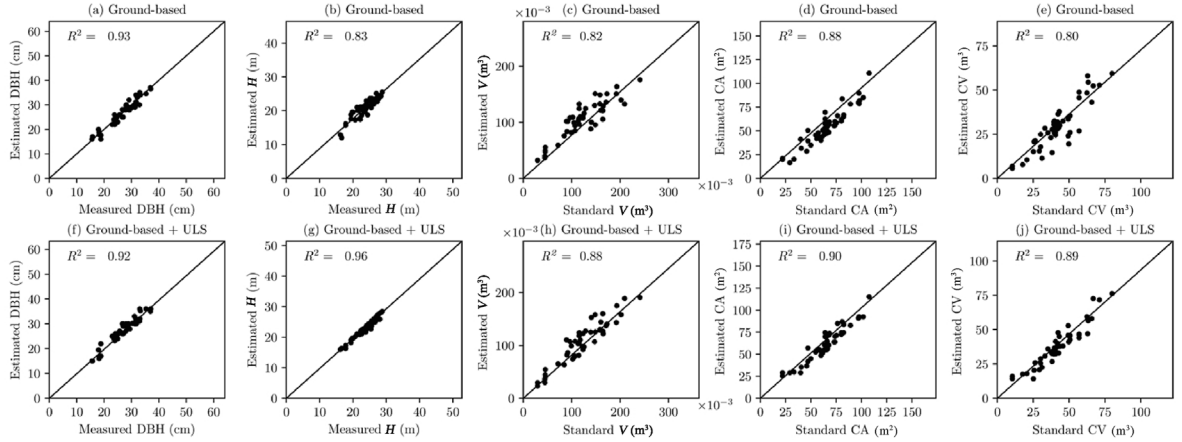

Fig. 17. Scatterplots of estimated tree parameters and field measurements of dawn redwood species. Top row: ground-based LiDAR data. Bottom row: fused point cloud.

(18.61%) based on *r*RMSE because of the clumped canopy. It can be concluded that ground-based/ULS LiDAR data fusion has strong potential for tree parameter estimation, particularly in dense canopies. It is worth noting that all of these benefits were based on single-flight ULS data. Thus, multiple-fight ULS data would be more beneficial to tree parameter estimation from ground-based/ULS LiDAR data fusion because higher tree levels (thinner trucks and branches) would be better reconstructed from higher-density point clouds.

Moreover, the performance of fusion-derived tree heights and ULS-derived tree heights were compared to the field measurements. For poplar trees, the *r*RMSE of ULS-derived *H* compared to reference field measurements was 3.96% while its counterpart from fusion was 3.76% which means that ULS-derived tree height did not significantly benefit from fusion. Similarly, the ULS-derived *H* of dawn redwood trees was not remarkably changed compared to fusion-derived *H* because their *r*RMSEs were 4.73% and 4.58%, respectively. This could be attributed to the ULS data collection perspective where the treetops and higher-canopy levels are effectively scanned from above however, the R^2 and *r*RMSE of fusion-derived *H* slightly outperformed those from ULS only by a maximum 0.04 and 0.2%, respectively as shown in Fig. 18.

According to Table 2, there was a large difference in point density between the ground-based dataset and ULS data. The tree structural modeling was greatly affected by the point density because the TreeQSM algorithm constructs the different tree segments based on the PatchDiameter 1 and 2. PatchDiameter2 determines the smallest tree element which can be modeled. Considering that trunks and branches account for the majority of tree volume, its improvement depends on how much trunk and branch volumes can be derived from ULS. Despite the ground-based/ULS data fusion, the tree volume has been improved by 5.28%. This could be attributed to the relatively low point density of ULS data which was not adequate to model the thin branches at high-tree levels. The crown volume has been calculated for the outer perimeter of the crown therefore, the ULS point density has been sufficient to model the surface shape of the crown. Consequently, the crown volume has significantly improved (18.61%) due to the ground-based/ULS data fusion.

Moreover, the LiDAR DEM accuracy is influenced by different factors including the sampling density of LiDAR, the morphological complexity of the terrain, the interpolation algorithm, and the land cover (Căeanu and Ciubotaru, 2021). The existence of dense shrubs downgrades the DEM accuracy because it prevents the well sampling of the ground-level due to the sensor penetration capability and the LiDAR samping density. It was proved that the DEM generation in case of near-flat terrain was not significantly affected by the existence of shrubs. In addition, in case of rough terrain topography, the shrubs effect on DEM generation can be reduced by lowering the flight altitude and narrowing the scan angle (Chen et al., 2022). Thus, the proposed registration method can be utilized in such situation using repeated-flight ULS at different scan angles at relatively low flight altitudes. In this study, the experiments included forest plots from a planted forest that had a near-flat terrain, so the effect of terrain and topography was not significant. Moreover, the ULS flight altitude was relatively low (86 m) thus enabled a sufficient

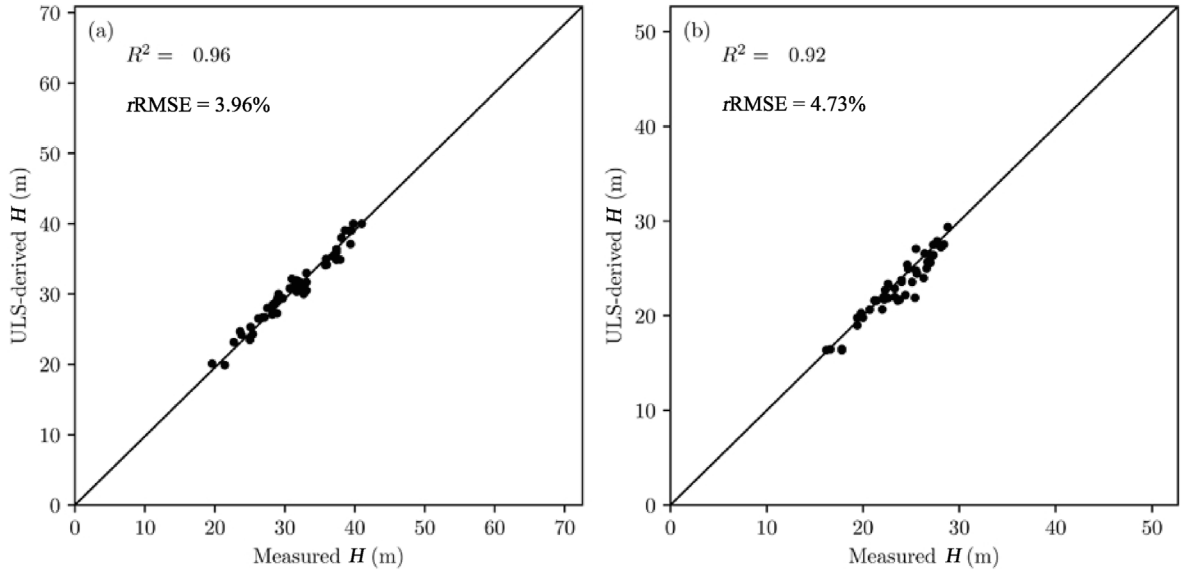

Fig. 18. Scatterplots of the ULS-derived heights versus field measurements. (**a**) Tree heights of poplar species. (**b**) Tree heights of dawn redwood species.

representation of the ground level.

From a dataset point of view, structural tree parameter estimation based on point clouds was performed using either photogrammetric point clouds from a UAV (Ye et al., 2019; Shimizu et al., 2022) or LiDAR point clouds (Brede et al., 2019; Terryn et al., 2022). For instance, Terryn et al. (2022) compared the DBH, *H*, CA, and CV of a tropical forest from TLS and ULS to TLS/ULS data fusion as a benchmark, with the exception of DBH (RMSE = 5.04 cm), which was compared to census data. This study also investigated the effect of single- and multiple-return ULS on parameter estimation. DBH and tree height were estimated based on least-squares circle fitting and height difference between the highest and lowest points of the tree point cloud, respectively. Their results were obtained for only the largest trees in all plots, and they did not report any improvements in *H*, CA, or CV owing to fusion. For instance, both TLS- and ULS-derived *H* reported a difference of $\leq$ 1% compared with the benchmark. Similarly, CA and CV did not record improvements for both TLS (RMSE: 3.06 m^2, 29.63 m^3) and ULS (RMSE: $<$ 5.5 m^2, 30.33 m^3). This can be attributed to the fact that they considered fusion-derived parameters as benchmark. By contrast, our fusion-derived *H* and CV showed remarkable improvements in terms of *r*RMSE of up to 9.01% and 18.61%, respectively, compared to real field data. Additionally, DBH was only estimated from the TLS data because stems were not sampled from the ULS dataset.

In addition, Shimizu et al. (2022) estimated the tree parameters from TLS and TLS/UAV-photogrammetric data fusion in a Japanese managed forest of coniferous species. DBH was estimated based on circle fitting, whereas *H* was estimated based on matching CHM-derived treetops with TLS tree locations. They reported that fusion-derived *H* was remarkably improved by 6.2%, whereas DBH was not estimated from fusion (TLS: *r*RMSE = 5.6%). Our findings are in line with these results because fusion-derived *H* was improved by 9.01%, and the *r*RMSE of DBH from ground-based LiDAR was 5.77% for dawn redwood (coniferous) trees. Our fusion-derived *H* outperformed because matching CHM-detected treetops and TLS tree locations might involve false matches, which affects the fusion and parameter estimation results. In addition, Ye et al. (2019) investigated the potential of UAV photogrammetric point clouds for the QSM of single trees to assess woody biomass in both leaf-on and leaf-off seasons. They collected data using an oblique camera to increase point density. Despite their promising results, which showed that the UAV point cloud could precisely estimate tree parameters, the biomass was underestimated by approximately 49%. Even with low-cost and large-scale data collection, the change in sunlight intensity and poor radiometric quality because of cloudy weather still pose major challenges. By contrast, owing to its penetration capability, the UAV-LiDAR can sense under-canopy levels; however, with a lower point density compared to higher canopy levels. Therefore, fusion with ground-based LiDAR systems is expected to not only improve data completeness but also increase the point density at the lower canopy level, which was achieved in our study. The fusion-derived *V* improved by up to 5.28%. Such improvement can be justified by the ground-based/ULS LiDAR data fusion, as the ULS enhanced the sampling of the high canopy level.

Moreover, Brede et al. (2019) compared the capability of ULS data in tree parameter estimation using *TreeQSM* to TLS. It was found that the trunks and branches of diameter $\geq$ 30 cm were modeled well using UAV-LiDAR with a RMSE of 1.12 m^3, whereas smaller branches led to volume overestimation by an average of 41.3%. The study showed the strong impact of clumped canopy on ULS-derived *V* because the tree trunk was characterized by sparse points with an increased RMSE by 6.6 m^3. Based on these findings, it is worth noting that structural modelling of single trees from ULS data of dense canopies was extremely challenging. Therefore, we used the fusion of UAV and ground-based LiDAR systems in our study for the precise representation of trees. Our results showed that the fusion-derived *V* improved (5.28%) in terms of *r*RMSE. Thus, ground-based/ULS LiDAR data fusion is required to complete and enhance point cloud representation, particularly in dense forest stands.

Tree height is a key contributor to the AGB estimation of single trees. A comparative study (Laurin et al., 2019) investigated the performance of ALS, TLS, and UAV photogrammetry point clouds for tree height estimation. They reported that tree height underestimation was expected from the three datasets owing to instrumental limitations and/or local forest conditions. They proposed that the integration of different systems would lead to a more rigorous estimation of the tree height. A similar finding was also corroborated in Liang et al. (2019) and Brede et al. (2017). In our study, the dawn redwood plots had a clumped canopy, and the fusion-derived *H* was improved by 9.01% in terms of *r*RMSE. Consequently, ground-based/ULS LiDAR data fusion is an effective solution for volume and/or tree height estimation in complex forest environments.

It is also worth noting that the experimental results were obtained in plantation forests with homogeneous forest structures, such as monotype tree species and principally equivalent tree attributes. By contrast, a natural forest preserves complex sample plots with mixed species and a wide variety of tree patterns and attributes. Such discrepancies would pose a critical challenge to the QSM of trees dependent on a single LiDAR

platform. For instance, understory trees cannot be sampled from the ULS point cloud, whereas treetops of large trees cannot be captured using ground-based LiDAR. Hence, tree parameter derivation based on ground-based/ULS LiDAR data fusion is of great importance, particularly for natural forests, where the fusion will reveal the entire 3D extent of the tree by compensating for the deficiency of individual platforms.

In addition, multi-layer forest is one type of high complexity to existing LiDAR data registration approaches particularly in case of ground-based/airborne LiDAR data integration. On the one hand, there will be many understory trees that are not expected to be extracted from airborne LiDAR date due to the sensor penetration capability and dense understory. Thus, the tree location matching between ground-based and airborne LiDAR data will be challenging because there are a lot of tree locations that have no counterparts in those from airborne LiDAR data. On the other hand, the extraction of virtual keypoints would be challenging in such forest type however the removal of under-canopy will decrease the number of understory trees before the keypoints extraction. Accordingly, only relatively high trees will be used for keypoints extraction based on canopy analysis to co-register the point cloud pair. However, the proposed method requires further investigations against such forest types.

7. Conclusions

In this study, a holistic framework for 3D tree modelling using ground-based/ULS LiDAR data fusion based on QSM was developed. In general, the use of virtual keypoints for co-registration significantly alleviated the limitations in tree localization, particularly in the case of ground-based/ULS LiDAR co-registration, where the stems were only identified appropriately from the ground-based LiDAR dataset. The experimental results of a subtropical plantation forest, including poplar and dawn redwood trees, showed that the fusion-derived *H*, *V*, and CV were remarkably improved, whereas DBH and CA were the least profited. Moreover, fusion-derived tree parameters of dawn redwood plots were significantly improved compared to those of poplar trees because of the relatively higher stem density of dawn redwood plots. Such improvements in the fusion-derived tree parameters, particularly tree height, would improve AGB estimation because tree height is a key contributor to AGB estimation. Such a fusion scheme can be further investigated in a more complex natural forest where there is a high variety of tree parameters at the plot level, which may include mixed tree species. This diversity provides an opportunity to further examine the performance of point-cloud fusion and biophysical parameter estimation.

Acknowledgment

This work was supported by the National Natural Science Foundation of China (Project No. 42171361), the Research Grants Council of the Hong Kong Special Administrative Region, China, under Project PolyU 25211819, and in part by the Hong Kong Polytechnic University under Projects 1-ZE8E and 1-ZVN6.

References

Béland, M., Baldocchi, D.D., Widlowski, J.L., Fournier, R.A., Verstraete, M.M., 2013. On seeing the wood from the leaves and the role of voxel size in determining leaf area distribution of forests with terrestrial LiDAR. Agric. For. Meteorol. 184, 82–97. https://doi.org/10.1016/j.agrformet.2013.09.005.

Belton, D., Moncrieff, S., Chapman, J., 2013. Processing tree point clouds using Gaussian Mixture Models. In: ISPRS Ann. Photogramm. Remote Sens. Spat. Inf. Sci. Volume II-5/W2. ISPRS Workshop Laser Scanning 2013, 11–13 November 2013, Antalya, Turkey, pp. 43–48. https://doi.org/10.5194/isprsannals-II-5-W2-43-2013.

Brede, B., Calders, K., Lau, A., Raumonen, P., Bartholomeus, H.M., Herold, M., Kooistra, L., 2019. Non-destructive tree volume estimation through quantitative structure modelling: comparing UAV laser scanning with terrestrial LIDAR. Remote Sens. Environ. 233, 111355. https://doi.org/10.1016/j.rse.2019.111355.

Brede, B., Lau, A., Bartholomeus, H.M., Kooistra, L., 2017. Comparing RIEGL RiCOPTER UAV LiDAR derived canopy height and DBH with terrestrial LiDAR. Sensors 17, 2371. https://doi.org/10.3390/s17102371.

Calders, K., Adams, J., Armston, J., Bartholomeus, H., Bauwens, S., Bentley, L.P., Chave, J., Danson, F.M., Demol, M., Disney, M., Gaulton, R., Krishna Moorthy, S.M., Levick, S.R., Saarinen, N., Schaaf, C., Stovall, A., Terryn, L., Wilkes, P., Verbeeck, H., 2020. Terrestrial laser scanning in forest ecology: expanding the horizon. Remote Sens. Environ. 251, 112102. https://doi.org/10.1016/j.rse.2020.112102.

Calders, K., Newnham, G., Burt, A., Murphy, S., Raumonen, P., Herold, M., Culvenor, D., Avitabile, V., Disney, M., Armston, J., Kaasalainen, M., 2015. Nondestructive estimates of above-ground biomass using terrestrial laser scanning. Methods Ecol. Evol. 6, 198–208. https://doi.org/10.1111/2041-210X.12301.

Campello, R.J.G.B., Moulavi, D., Sander, J., 2013. Density-based clustering based on hierarchical density estimates. In: Pei, J., Tseng, V.S., Cao, L., Motoda, H., Xu, G. (Eds.), Advances in Knowledge Discovery and Data Mining. PAKDD 2013. Lecture Notes in Computer Science, vol 7819. Springer, Berlin, Heidelberg, pp. 160–172. https://doi.org/10.1007/978-3-642-37456-2_14.

Căeanu, M., Ciubotaru, A., 2021. The effect of LiDAR sampling density on DTM accuracy for areas with heavy forest cover. Forests 12, 265. https://doi.org/10.3390/f12030265.

Chen, Q., Gao, T., Zhu, J., Wu, F., Li, X., Lu, D., Yu, F., 2022. Individual tree segmentation and tree height estimation using leaf-off and leaf-on UAV-LiDAR data in dense deciduous forests. Rem. Sens. 14. https://doi.org/10.3390/rs14122787.

Corte, A.P.D., Rex, F.E., de Almeida, D.R.A., Sanquetta, C.R., Silva, C.A., Moura, M.M., Wilkinson, B., Zambrano, A.M.A., da Cunha Neto, E.M., Veras, H.F.P., de Moraes, A., Klauberg, C., Mohan, M., Cardil, A., Broadbent, E.N., 2020. Measuring individual tree diameter and height using GatorEye high-density UAV-lidar in an integrated crop-livestock-forest system. Rem. Sens. 12, 863. https://doi.org/10.3390/rs12050863.

Dai, W., Yang, B., Liang, X., Dong, Z., Huang, R., Wang, Y., Li, W., 2019. Automated fusion of forest airborne and terrestrial point clouds through canopy density analysis. ISPRS J. Photogrammetry Remote Sens. 156, 94–107. https://doi.org/10.1016/j.isprsjprs.2019.08.008.

Delagrange, S., Jauvin, C., Rochon, P., 2014. PypeTree: a tool for reconstructing tree perennial tissues from point clouds. Sensors 14, 4271–4289. https://doi.org/10.3390/s140304271.

FAO, UNEP, 2020. The State of the World's Forests 2020. Forests, biodiversity and people, Rome. https://doi.org/10.4060/ca8642en.

Fekry, R., Yao, W., Cao, L., Shen, X., 2021. Marker-less UAV-LiDAR strip alignment in plantation forests based on topological persistence analysis of clustered canopy cover. ISPRS Int. J. Geo-Inf. 10. https://doi.org/10.3390/ijgi10050284.

Gao, S., Zhang, Z., Cao, L., 2021. Individual tree structural parameter extraction and volume table creation based on near-field LiDAR data: a case study in a subtropical planted forest. Sensors 21, 8162. https://doi.org/10.3390/s21238162.

Gonzalez de Tanago, J., Lau, A., Bartholomeus, H., Herold, M., Avitabile, V., Raumonen, P., Martius, C., Goodman, R.C., Disney, M., Manuri, S., Burt, A., Calders, K., 2018. Estimation of above-ground biomass of large tropical trees with terrestrial LiDAR. Methods Ecol. Evol. 9, 223–234. https://doi.org/10.1111/2041-210X.12904.

Guan, H., Su, Y., Hu, T., Wang, R., Ma, Q., Yang, Q., Sun, X., Li, Y., 2019. A novel framework to automatically fuse multiplatform LiDAR data in forest environments based on tree locations. IEEE Trans. Geosci. Rem. Sens. 58, 2165–2177. https://doi.org/10.1109/TGRS.2019.2953654.

Guo, Q., Li, W., Yu, H., Alvarez, O., 2010. Effects of topographic variability and lidar sampling density on several DEM interpolation methods. Photogramm. Eng. Rem. Sens. 76, 701–712.

Hackenberg, J., Spiecker, H., Calders, K., Disney, M., Raumonen, P., 2015. SimpleTree - an efficient open source tool to build tree models from TLS clouds. Forests 6, 4245–4294. https://doi.org/10.3390/f6114245.

Hu, S., Li, Z., Zhang, Z., He, D., Wimmer, M., 2017. Efficient tree modeling from airborne LiDAR point clouds. Comput. Graph. 67, 1–13. https://doi.org/10.1016/j.cag.2017.04.004.

Hyyppä, E., Kukko, A., Kaijaluoto, R., White, J.C., Wulder, M.A., Pyörälä, J., Liang, X., Yu, X., Wang, Y., Kaartinen, H., Virtanen, J.P., Hyyppä, J., 2020. Accurate derivation of stem curve and volume using backpack mobile laser scanning. ISPRS J. Photogrammetry Remote Sens. 161, 246–262. https://doi.org/10.1016/j.isprsjprs.2020.01.018.

Kalwar, O.P.P., Hussin, Y.A., Weir, M.J.C., de Bie, C., Karna, Y., 2021. Deriving forest plot inventory parameters using terrestrial laser scanning in the tropical rainforest of Malaysia. Int. J. Rem. Sens. 42, 884–901. https://doi.org/10.1080/01431161.2020.1817606.

Kelbe, D., Van Aardt, J., Romanczyk, P., Van Leeuwen, M., Cawse-Nicholson, K., 2016. Multiview marker-free registration of forest terrestrial laser scanner data with embedded confidence metrics. IEEE Trans. Geosci. Rem. Sens. 55, 729–741. https://doi.org/10.1109/TGRS.2016.2614251.

Ko, C., Lee, S., Yim, J., Kim, D., Kang, J., 2021. Comparison of forest inventory methods at plot-level between a backpack personal laser scanning (BLPS) and conventional equipment in Jeju Island, South Korea. Forests 12. https://doi.org/10.3390/f12030308.

Lau, A., Bentley, L.P., Martius, C., Shenkin, A., Bartholomeus, H., Raumonen, P., Malhi, Y., Jackson, T., Herold, M., 2018. Quantifying branch architecture of tropical trees using terrestrial LiDAR and 3D modelling. Trees (Berl.) 32, 1219–1231. https://doi.org/10.1007/s00468-018-1704-1.

Laurin, G.V., Ding, J., Disney, M., Bartholomeus, H., Herold, M., Papale, D., Valentini, R., 2019. Tree height in tropical forest as measured by different ground, proximal, and remote sensing instruments, and impacts on above ground biomass estimates. Int. J. Appl. Earth Obs. Geoinf. 82, 101899. https://doi.org/10.1016/j.jag.2019.101899.

Li, W., Guo, Q., Jakubowski, M.K., Kelly, M., 2012. A new method for segmenting individual trees from the LiDAR point cloud. Photogramm. Eng. Rem. Sens. 78, 75–84. https://doi.org/10.14358/PERS.78.1.75.

Liang, X., Wang, Y., Pyörälä, J., Lehtomäki, M., Yu, X., Kaartinen, H., Kukko, A., Honkavaara, E., Issaoui, A.E.I., Nevalainen, O., Vaaja, M., Virtanen, J.P., Katoh, M., Deng, S., 2019. Forest in situ observations using unmanned aerial vehicle as an alternative of terrestrial measurements. For. Ecosyst. 6, 20. https://doi.org/10.1186/s40663-019-0173-3.

Moorthy, S.M.K., Calders, K., Vicari, M.B., Verbeeck, H., 2020. Improved supervised learning-based approach for leaf and wood classification from LiDAR point clouds of forests. IEEE Trans. Geosci. Rem. Sens. 58, 3057–3070. https://doi.org/10.1109/TGRS.2019.2947198.

Navarro, A., Young, M., Allan, B., Carnell, P., Macreadie, P., Ierodiaconou, D., 2020. The application of Unmanned Aerial Vehicles (UAVs) to estimate above-ground biomass of mangrove ecosystems. Remote Sens. Environ. 242, 111747. https://doi.org/10.1016/j.rse.2020.111747.

Ning, X., Li, F., Tian, G., Wang, Y., 2018. An efficient outlier removal method for scattered point cloud data. PLoS One 13, 1–22. https://doi.org/10.1371/journal.pone.0201280.

Oveland, I., Hauglin, M., Giannetti, F., Kjørsvik, N.S., Gobakken, T., 2018. Comparing three different ground based laser scanning methods for tree stem detection. Rem. Sens. 10, 1–17. https://doi.org/10.3390/rs10040538.

Paris, C., Kelbe, D., Van Aardt, J., Bruzzone, L., 2017. A novel automatic method for the fusion of ALS and TLS LiDAR data for robust assessment of tree crown structure. IEEE Trans. Geosci. Rem. Sens. 55, 3679–3693. https://doi.org/10.1109/TGRS.2017.2675963.

Pitkänen, T.P., Raumonen, P., Kangas, A., 2019. Measuring stem diameters with TLS in boreal forests by complementary fitting procedure. ISPRS J. Photogrammetry Remote Sens. 147, 294–306. https://doi.org/10.1016/j.isprsjprs.2018.11.027.

Polewski, P., Erickson, A., Yao, W., Coops, N., Krzystek, P., Stilla, U., 2016. Object-based coregistration of terrestrial photogrammetric and ALS point clouds in forested areas. In: ISPRS Ann. Photogramm. Remote Sens. Spat. Inf. Sci., pp. 347–354. https://doi.org/10.5194/isprs-annals-III-3-347-2016.

Polewski, P., Yao, W., 2019. Scale invariant line-based co-registration of multimodal aerial data using L1 minimization of spatial and angular deviations. ISPRS J. Photogrammetry Remote Sens. 152, 79–93. https://doi.org/10.1016/j.isprsjprs.2019.04.004.

Polewski, P., Yao, W., Cao, L., Gao, S., 2019. Marker-free coregistration of UAV and backpack LiDAR point clouds in forested areas. ISPRS J. Photogrammetry Remote Sens. 147, 307–318. https://doi.org/10.1016/j.isprsjprs.2018.11.020.

Raumonen, P., Kaasalainen, M., Markku, Å., Kaasalainen, S., Kaartinen, H., Vastaranta, M., Holopainen, M., Disney, M., Lewis, P., 2013. Fast automatic precision tree models from terrestrial laser scanner data. Rem. Sens. 5, 491–520. https://doi.org/10.3390/rs5020491.

Shimizu, K., Nishizono, T., Kitahara, F., Fukumoto, K., Saito, H., 2022. Integrating terrestrial laser scanning and unmanned aerial vehicle photogrammetry to estimate individual tree attributes in managed coniferous forests in Japan. Int. J. Appl. Earth Obs. Geoinf. 106, 102658. https://doi.org/10.1016/j.jag.2021.102658.

Stovall, A.E.L., Vorster, A.G., Anderson, R.S., Evangelista, P.H., Shugart, H.H., 2017. Non-destructive aboveground biomass estimation of coniferous trees using terrestrial LiDAR. Remote Sens. Environ. 200, 31–42. https://doi.org/10.1016/j.rse.2017.08.013.

Tao, S., Wu, F., Guo, Q., Wang, Y., Li, W., Xue, B., Hu, X., Li, P., Tian, D., Li, C., Yao, H., Li, Y., Xu, G., Fang, J., 2015. Segmenting tree crowns from terrestrial and mobile LiDAR data by exploring ecological theories. ISPRS J. Photogrammetry Remote Sens. 110, 66–76. https://doi.org/10.1016/j.isprsjprs.2015.10.007.

Terryn, L., Calders, K., Bartholomeus, H., Bartolo, R.E., Brede, B., D'hont, B., Disney, M., Herold, M., Lau, A., Shenkin, A., Whiteside, T.G., Wilkes, P., Verbeeck, H., 2022. Quantifying tropical forest structure through terrestrial and UAV laser scanning fusion in Australian rainforests. Rem. Sens. Environ. 271, 112912. https://doi.org/10.1016/j.rse.2022.112912.

Wan, P., Wang, T., Zhang, W., Liang, X., Skidmore, A.K., Yan, G., 2019. Quantification of occlusions influencing the tree stem curve retrieving from single-scan terrestrial laser scanning data. For. Ecosyst. 6, 43. https://doi.org/10.1186/s40663-019-0203-1.

Wang, Y., Pyörälä, J., Liang, X., Lehtomäki, M., Kukko, A., Yu, X., Kaartinen, H., Hyyppä, J., 2019. In situ biomass estimation at tree and plot levels: what did data record and what did algorithms derive from terrestrial and aerial point clouds in boreal forest. Rem. Sens. Environ. 232, 111309. https://doi.org/10.1016/j.rse.2019.111309.

Wang, Z., Zhang, L.L., Zhang, L., Li, R., Zheng, Y., Zhu, Z., 2018. A deep neural network with spatial pooling (DNNSP) for 3-D point cloud classification. IEEE Trans. Geosci. Rem. Sens. 56, 4594–4604. https://doi.org/10.1109/TGRS.2018.2829625.

Xu, S., Zhou, K., Sun, Y., Yun, T., 2021. Separation of wood and foliage for trees from ground point clouds using a novel least-cost path model. IEEE J. Sel. Top. Appl. Earth Obs. Rem. Sens. 14, 6414–6425. https://doi.org/10.1109/jstars.2021.3090502.

Yao, W., Krzystek, P., Heurich, M., 2012. Tree species classification and estimation of stem volume and DBH based on single tree extraction by exploiting airborne full-waveform LiDAR data. Rem. Sens. Environ. 123, 368–380. https://doi.org/10.1016/j.rse.2012.03.027.

Ye, N., van Leeuwen, L., Nyktas, P., 2019. Analysing the potential of UAV point cloud as input in quantitative structure modelling for assessment of woody biomass of single trees. Int. J. Appl. Earth Obs. Geoinf. 81, 47–57. https://doi.org/10.1016/j.jag.2019.05.010.

Zhang, C., Jiang, Y., Xu, B., Li, X., Zhu, Y., Lei, L., Chen, R., Dong, Z., Yang, H., Yang, G., Jiang, Y., Xu, B., Li, X., Zhu, Y., Lei, L., Chen, R., Dong, Z., Yang, H., 2020. Apple tree branch information extraction from terrestrial laser scanning and backpack-LiDAR. Rem. Sens. 12, 1–17. https://doi.org/10.3390/rs12213592.